Acta Pharmaceutica Sinica B 2023;13(2):559−576

Chinese Pharmaceutical Association
Institute of Materia Medica, Chinese Academy of Medical Sciences

Acta Pharmaceutica Sinica B

www.elsevier.com/locate/apsb
www.sciencedirect.com

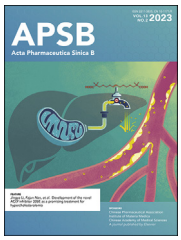

ORIGINAL ARTICLE

# SIRT1 activation synergizes with FXR agonism in hepatoprotection *via* governing nucleocytoplasmic shuttling and degradation of FXR

**Shuang Cui, Huijian Hu, An Chen, Ming Cui, Xiaojie Pan, Pengfei Zhang, Guangji Wang, Hong Wang*, Haiping Hao***

*State Key Laboratory of Natural Medicines, Key Laboratory of Drug Metabolism & Pharmacokinetics, China Pharmaceutical University, Nanjing 210009, China*

Received 26 April 2022; received in revised form 28 June 2022; accepted 28 July 2022

**KEY WORDS**

FXR;
Nuclear receptor;
Acetylation;
Phosphorylation;
Nucleocytoplasmic shuttling;
Degradation;
Nonalcoholic steatohepatitis;
Combinatorial drugs

**Abstract** Farnesoid X receptor (FXR) is widely accepted as a promising target for various liver diseases; however, panels of ligands in drug development show limited clinical benefits, without a clear mechanism. Here, we reveal that acetylation initiates and orchestrates FXR nucleocytoplasmic shuttling and then enhances degradation by the cytosolic E3 ligase CHIP under conditions of liver injury, which represents the major culprit that limits the clinical benefits of FXR agonists against liver diseases. Upon inflammatory and apoptotic stimulation, enhanced FXR acetylation at K217, closed to the nuclear location signal, blocks its recognition by importin KPNA3, thereby preventing its nuclear import. Concomitantly, reduced phosphorylation at T442 within the nuclear export signals promotes its recognition by exportin CRM1, and thereby facilitating FXR export to the cytosol. Acetylation governs nucleocytoplasmic shuttling of FXR, resulting in enhanced cytosolic retention of FXR that is amenable to degradation by CHIP. SIRT1 activators reduce FXR acetylation and prevent its cytosolic degradation. More importantly, SIRT1 activators synergize with FXR agonists in combating acute and chronic liver injuries. In conclusion, these findings innovate a promising strategy to develop therapeutics against liver diseases by combining SIRT1 activators and FXR agonists.

*Corresponding authors. Tel./fax.: +86 025 83271179 (Haiping Hao), +86 025 83271176 (Hong Wang).
E-mail addresses: haipinghao@cpu.edu.cn (Haiping Hao), wanghong@cpu.edu.cn (Hong Wang).

Peer review under the responsibility of Chinese Pharmaceutical Association and Institute of Materia Medica, Chinese Academy of Medical Sciences.

https://doi.org/10.1016/j.apsb.2022.08.019

## 1. Introduction

Nonalcoholic fatty liver disease (NAFLD) is currently regarded as the most common liver disease worldwide, and more than 25% of the world population suffers from NAFLD. Despite its high prevalence worldwide, there are currently no pharmaceutical therapeutics approved for NAFLD and its progressive subtype, nonalcoholic steatohepatitis (NASH), highlighting the urgent to develop effective medicines[1].

Farnesoid X receptor (FXR), a typical nuclear receptor (NR), has now been widely exploited for developing drugs against various diseases, particularly NASH[2,3]. Compelling preclinical evidence suggest its pleiotropic effects on metabolic regulation[4,5], inflammation suppression[6,7], cell death prevention[8,9], and fibrogenesis inhibition[10,11]. Therefore, numerous FXR agonists with diverse chemical structures have been developed[12]. Among the proposed FXR agonists, obeticholic acid (OCA) seems to be particularly promising. Recently, OCA achieved endpoints in a phase III clinical trial for NASH[13]. Although the study was the first phase III clinical trial for NASH to show a benefit, some questions remain[14]. One of the main concerns is the limited clinical benefit of OCA. Although the co-primary endpoint of fibrosis improvement was achieved, the response rate was low, and the co-primary endpoint of NASH resolution was not achieved[13]. Hence, the approval of OCA for NASH therapy has been delayed by FDA. Besides, other FXR agonists in clinical trials are also pessimistic about their prospective as drug candidates against NASH. The clinical evidence has dampened enthusiasm for FXR agonists in NASH therapy and suggests that there is still a gap in knowledge about FXR biology in liver diseases. Hence, it is critical to uncover the underlying mechanisms associated with limited efficacy of FXR agonists in patients suffer from liver diseases.

We have previously observed reduced hepatic FXR protein levels in fibrotic patients accompanied with the progress of fibrosis development[8]; this was also observed in patients with NASH and primary biliary cirrhosis[15,16]. Most biological functions of FXR rely on its transcriptional regulation of target genes in the nucleus, which is stimulated when agonists bind to the pocket of FXR protein. According to the "occupancy-driven" mechanism of action, it is reasonable to predict that the enhanced degradation of FXR protein in conditions of liver injury would likely represent the key to explain the limited clinical benefits of FXR agonists. Thus, it is of paramount importance to clarify the way and mechanism underlying the facilitated FXR protein degradation in conditions of liver diseases. To this end, we sought to delineate the precise mechanisms underlying FXR degradation in liver diseases.

NRs, of course including FXR, are believed to mainly localize and function in nuclear compartment[17,18]. In addition to functional fulfillment, degradation of cellular proteins *via* either the ubiquitin-proteasome system (UPS) or autophagy occurs in a compartment-specific manner[19]. Although the nucleus has been identified as a compartment for protein degradation[20], the cytosol is the prominent compartment for intracellular protein degradation[21,22]. In contrast to cytosolic degradation of aboriginal proteins, degradation of nuclear proteins in the cytosol poses significant topological problems. Hence, the shuttling of nuclear proteins between these two compartments is essential for their cytosolic degradation. Proteins larger than 40 kDa that shuttle between the cytosol and nucleus must bind to import/export receptors, and to achieve this, they must possess the nuclear location signal (NLS)/nuclear export signal (NES), respectively. However, how these signals are critically regulated to induce nuclear export for cytosolic degradation of NRs and, in particular, the precise mechanism underlying the coupling of nucleocytoplasmic shuttling with protein degradation remain largely uncharacterized. We found that acetylation orchestrates the nucleocytoplasmic shuttling and protein degradation of FXR. Furthermore, we showed that SIRT1 activators synergize with FXR agonists for hepatoprotection against acute and chronic liver injuries in preclinical mouse models.

## 2. Materials and methods

### 2.1. Reagents

Actinomycin D (HY-17559), EX527 (HY-1545), MG132 (HY-13259), obeticholic acid (HY-12222), SRT1720 hydrochloride (HY-15145) and tropifexor (HY-107418) were purchased from MedChemExpress. Cycloheximide (HY-12320), nicotinamide (98-92-0) and dimethyl sulfoxide (67-68-5) were purchased from Sigma−Aldrich. DAPI staining solution (C1005), leptomycin B (S1726) and trichostatin A (S1893) were purchased from Beyotime. Recombinant human TNF$\alpha$ (300-01 A) was purchased from Peprotech. Recombinant human FasL (10,244-H07Y) and recombinant human TRAIL (10409-HNAE) were purchased from Sino Biological. Recombinant murine TNF$\alpha$ (14-8321-63) was purchased from Bioworld Technology.

### 2.2. Animal treatment

Male C57BL/6 J mice (6 weeks old, 20 g) were obtained from Vital River Laboratory Animal Technology Co., Ltd. (Beijing, China). All mice were kept in an air-conditioned animal quarter at a temperature of 25 ± 2 °C and a relative humidity of 50 ± 10% with 12-h light/dark cycles for 1 week before experiments, and allowed water and standard chow ad libitum. All the animal studies were approved by the Animal Ethics Committee of China Pharmaceutical University (Nanjing, China).

To compare the hepatic FXR expression in healthy and liver injured mice, various murine models were induced. Acute liver injury was induced by intraperitoneal (i.p.) injection of $CCl_4$ (20% $CCl_4$ diluted in mineral oil; five mL/kg). Cholestatic liver injury was induced by bile duct ligation (BDL) as previously described[6]. NASH was induced either by high fat & high cholesterol diet (HFHC, 40% fat and 0.2% cholesterol in diet, and fructose/

sucrose at 23.1/18.9 g/L in drinking water) for 16 weeks or methionine and choline-deficient diet (MCD, from Trophic Animal Feed High-tech Co., Ltd.) for 6 weeks.

To evaluate the effect of FXR loss on the hepatoprotective effects of OCA, mice were intravenously (i.v.) injected with AAV Ctrl shRNA or AAV *Fxr* shRNA ($10^{11}$ vg/mouse). Two months later, these mice were orally administrated with vehicle or OCA (5 mg/kg/day) for 2 days. One hour after the last dosage of OCA, mice were injected (i.p.) with $CCl_4$ as above mentioned. Forty-eight hours later, mice were sacrificed. To further evaluate the effect of FXR loss caused by liver injury on the benefits of OCA, mice were injected (i.p.) with vehicle or $CCl_4$. Twenty-four hours later, mice were orally administrated with vehicle or OCA (5 mg/kg/day) for 2 days. Twenty-four hours after the last dosage of OCA, mice were sacrificed. To further confirm the effect of FXR expression on the benefits of OCA, mice were injected (i.v.) with Ad-Ctrl or Ad-*Fxr* ($10^9$ pfu/mouse). Five days later, these mice were injected with vehicle or $CCl_4$ (20% $CCl_4$ diluted in mineral; five mL/kg). Twenty-four hours later, mice were orally administrated with vehicle or OCA (5 mg/kg/day) for 2 days. Twenty-four hours after the last dosage of OCA, mice were sacrificed.

To investigate the effect of co-administration of OCA and SRT1720 on liver injuries, mice were injected with $CCl_4$ or fed with HFHC diet as described above. Mice were injected (i.p.) with SRT1720 (10 mg/kg/day, twice daily) for 5 days. Mice were injected (i.p.) with $CCl_4$ (20% $CCl_4$ diluted in mineral; five mL/kg) at the 3rd day and orally administrated with OCA (1.5 and 5 mg/kg/day) for 2 days from the 4th day since SRT1720 treatment. Seventy-two hours after $CCl_4$ injection, mice were sacrificed. Additionally, mice were fed with HFHC for 16 weeks to induce NASH. Mice were injected (i.p.) with SRT1720 (10 mg/kg/day, once daily) from the 12th week and orally administrated with OCA (1.5 and 5 mg/kg/day) from the 13th week.

### 2.3. Serum biochemical analysis

Serum levels of alanine aminotransferase (ALT) and aspartate aminotransferase (AST) were measured with commercial kits (Nanjing Jiancheng Bioengineering Institute, Nanjing, China) following the manufacturer's instructions.

### 2.4. Histological evaluation

Formalin-fixed hepatic tissues were embedded in paraffin and 5 μm-thick sections were cut for histological evaluation. Assessment of morphology and extracellular matrix accumulation were performed by hematoxylin and eosin (H&E) staining, Sirius red staining and Masson's trichrome staining. Evaluation of hepatic FXR expression was conducted by immunohistochemistry with an FXR antibody.

### 2.5. Cell lines and cell treatment

Human HepG2 cells, murine AML12 cells, and human HEK293T cells were obtained from Stem Cell Bank of the Chinese Academy of Sciences. HepG2 cells and HEK293 cells were cultured in Dulbecco's modified Eagle's medium (DMEM) containing 10% fetal bovine serum (FBS). AML12 cells were cultured in DMEM/F12 containing 10% FBS. These cell lines are mycoplasma free. Apoptosis was induced by following methods: (1) ActD (0.4 μmol/L)/TNFα (20 ng/mL); (2) CHX (50 μmol/L)/FasL (50 ng/mL); (3) TRAIL (50 ng/mL) for indicated time. Inflammation was induced by TNFα (100 ng/mL) for indicated time.

### 2.6. Cell viability by CCK-8 assay

Cells were grown in 96-well plates for cell viability by Cell Counting Kit-8 assay (CCK-8, Vazyme) following the protocol. Briefly, 10 μL of CCK-8 solution was added to each well of the plate before incubation at 37 °C for 1 h. The absorbance at 450 nm was read using a microplate reader.

### 2.7. Determination of apoptosis by flow cytometry

Apoptosis of HepG2 cells was determined using the Annexin V-FITC/Propidium Iodide kit (PI, BD Biosciences). Briefly, cells were trypsinized, washed, and suspended in annexin-binding buffer before stained with annexin V-FITC and PI for 20 min in the dark. The cells were then analyzed on a BD FACS Calibur (BD Bioscience) flow cytometer.

### 2.8. Plasmids and siRNA

Human *KPNA3* CRISPR/Cas9 KO plasmid were purchased from Santa cruz. Human *CHIP* (WT, H260Q), *Flag-SIRT1* were purchased from Sangon Biotech. Human *GFP-FXR* (WT, K217R, K217Q, T442A, T442E), *Flag-FXR* (WT, ΔAF1, ΔDBD, ΔHinge, ΔLBD), *GFP-FXR-NLS-GST*, *GFP-FXR-NLSm-GST*, *GFP-FXR-NLS (K217R)-GST*, *GFP-FXR-NLS (K217Q)-GST*, *GFP-FXR-NLS-NES1-GST*, *GFP-FXR-NLS-NES1m-GST*, *GFP-FXR-NLS-NES2-GST, GFP-FXR-NLS-NES2m-GST*, *GFP-FXR-NLS-NES (T442A)-GST*, *GFP-FXR-NLS-NES (T442E)-GST* and *Flag-CHIP* (WT, ΔTPR, ΔU-Box) were purchased from Jinzai Bio. Mouse adenovirus FXR were purchased from Viraltherapy Technologies.

Human *CRM1* siRNA (sc-35116), *CRT* siRNA (sc-29234) and silencer negative control siRNA (sc-37007) were purchased from Santa Cruz. Human *BARD1* siRNA designed as sequence *5′*-GGAUACAAGACUUGAAGAUTT-*3′* and *3′*-AUCUUCAAGUCUUGUAUCCTT-*5′*, *SMURF1* siRNA designed as sequence *5′*-UGAUCUAUAUGUUGGGAAATT-*3′* and *3′*-UUUCCCAACAUAUAGAUCATT-*5′*, *NEDD4* siRNA designed as sequence *5′*-CUAACAGAUGCUGAGAAUTT-*3′* and *3′*-AUUCUCAGCAUCUGUUAGGTT-*5′*, *ITCH* siRNA designed as sequence *5′*-GAGCAAUGCAGCAGUUUAATT-*3′* and *3′*-UUAAACUGCUGCAUUGCUCTT-*5′*, and *CHIP* siRNA designed as sequence *5′*-UGGCUAUGAAGGAGGUUAUTT-*3′* and *3′*-AUAACCUCCUUCAUAGCCATT-*5′* were obtained from EKBIO Technology. Human *SIRT1* siRNA designed as sequence *5′*-UCAUAGAGCCAUGAAGUAUGACAAA-*3′* and 3′-AGUAUCUCGGUACUUCAUACUGUUU-5′ were obtained from Invitrogen. Mouse AAV *Fxr* shRNA was purchased from Viraltherapy Technologies.

### 2.9. Plasmids and siRNA transfection

For plasmid transfection studies, the cells were transfected with control, Flag-FXR WT/mutants, Flag-CHIP WT/mutants, CHIP WT/mutants, GFP-FXR WT/mutants, Flag-SIRT1, GFP-NLS Cargo using Lipofectamine 3000 reagent (Invitrogen) according to the manufacturer's protocols.

For siRNA transfection studies, the cells were transfected with control siRNA, *NEDD4* siRNA, *ITCH* siRNA, *CHIP* siRNA, *BARD1* siRNA, *SMURF1* siRNA (Nanjing EKBIO Technology),

*CRM1* siRNA (Santa Cruz), *SIRT1* siRNA (Invitrogen) using lipofectamine RNAiMAX reagent (Invitrogen) for 48 h before ActD/TNF$\alpha$ treatment, according to the manufacturer's protocols.

### 2.10. Real-time PCR

Real-time PCR was performed following the previously reported protocols[23]. Briefly, total RNA was isolated from hepatic tissues or cells using RNAiso Plus reagent (TaKaRa Biotechnology). Purified RNA was reverse transcribed using PrimeScript RT Reagent Kit with gDNA Eraser (TaKaRa Biotechnology). Real-time PCR was performed with ChamQ SYBR qPCR Master Mix (Vazyme). Primer sequences are list in Supporting Information Table S1.

### 2.11. Antibodies

Anti-FXR (Abcam, 235,094, 1:750 for IHC; CST, 72,105, 1:1000 for WB; Santa Cruz, 25,309, 1:100 for IP; ABclonal, A8320, 1:200 for IF/PLA), anti-acetylated-lysine (CST, 9441, 1:1000), anti-phospho-threonine (CST, 9386, 1:1000), anti-ubiquitin (E4I2J) (CST, 91,112, 1:1000), anti-CHIP (CST, 2080, 1:1000), anti-histone H3 (CST, 4499, 1:1000), anti-$\beta$-actin (CST, 3700, 1:1000), anti-P300 (Santa Cruz, 48,343, 1:200), anti-BARD1 (ABclonal, A1685, 1:1000), anti-CRM1 (ABclonal, A19625, 1:1000), anti-ITCH (ABclonal, A8624, 1:1000), anti-MDM2 (ABclonal, A13327, 1:1000), anti-SMURF1 (ABclonal, A16559, 1:1000), anti-UBE4B (ABclonal, A17609, 1:1000), anti-KPNA1 (ABclonal, A1742, 1:1000), anti-KPNA2 (ABclonal, A1623, 1:1000), anti-KPNA3 (ABclonal, A8347, 1:1000), anti-KPNA4 (ABclonal, A2026, 1:1000), anti-KPNA5 (ABclonal, A7331, 1:1000), anti-KPNA6 (ABclonal, A7363, 1:1000), anti-SIRT1 (ABclonal, A11267, 1:1000), anti-calreticulin (Proteintech, 10292-1-AP, 1:1000), anti-GST-Tag (Proteintech, 10000-0-AP, 1:1000), anti-Flag-Tag (Abways, AB0008, 1:1000) and anti-GAPDH (Abways, AB0037, 1:1000) antibodies were used. Secondary antibodies, including goat anti-mouse IgG (H + L) antibody, HRP conjugated (Abcam, ab6789, 1:5000), goat anti-rabbit IgG (H + L) antibody, HRP conjugated (Abcam, ab6721, 1:5000), VeriBlot for IP detection reagent (HRP; Abcam, ab131366, 1:200), donkey anti-mouse IgG (H + L) Antibody, Alexa Fluor 555 (Invitrogen, A-31570, 1:2000) and donkey anti-rabbit IgG (H + L) antibody, Alexa Fluor 488 (Invitrogen, A-21206, 1:2000) were used.

### 2.12. Western blot

Western blot assays were performed following the previously reported protocols[24]. Briefly, protein lysates were separated by SDS−PAGE and transferred to a PVDF membrane, which was then blocked in 5% nonfat milk. The blots were incubated with primary antibodies and appropriate secondary antibodies, and detected by Enhanced Chemiluminescence Kit (ThermoFisher Scientific). Western blot acquisition was performed using iBright Analysis Software Version 3.0.1 (Thermo Fisher Scientific).

### 2.13. Cell fractionation assay

The cell nucleus and cytoplasm were isolated using the Nuclei Isolation Kit (Beyotime Biotechnology) according to the manufacturer's instructions. Cell fractionation were then analyzed by Western blot analysis as described above.

### 2.14. Co-immunoprecipitation (Co-IP) assay

Cells or tissues were lysed in chilled NP-40 buffer containing 1% protease inhibitor cocktail, and the lysates were immunoprecipitated with specific antibody together with Protein A-agarose (Invitrogen). The immune-precipitates were eluted from beads, resuspended in loading buffer, and then separated on SDS-PAGE gel, followed by Western blot analysis.

### 2.15. GST pull-down assay

GST pull-down assay was performed using Pierce GST Protein Interaction Pull-Down Kit (Thermo Scientific). GST-FXR protein or GST-KPNA3 protein coupled to Glutathione-Sepharose resin was mixed with appropriate HEK293T cell lysates overnight at 4 °C. The input and output samples were boiled in loading buffer and loaded on SDS-PAGE gels for separation and immunoblotting.

### 2.16. Immunofluorescence microscopy

HepG2 cells were seeded in cell imaging dish and fixed with 4% paraformaldehyde solution, followed by permeabilization with 0.2% Triton X-100. Cells were then incubated in blocking buffer and primary antibodies. After incubated with Alexa Fluor-conjugated secondary antibodies and DAPI, the cells were analyzed using a Zeiss 710 confocal microscope.

### 2.17. Ubiquitination assay

Cells were transiently transfected with different constructs as indicated in the text and figure captions and pre-treated with 5 μmol/L MG132 for 3 h. The cells were then lysed in lysis buffer containing protease inhibitor cocktail, *N*-ethylmaleimide, and iodoacetamide to preserve ubiquitin chains. *In vitro* ubiquitination assay using immunoprecipitation with anti-ubiquitin was performed as described above.

### 2.18. Bio-layer interferometry (BLI) assay

Direct protein−protein interactions were evaluated by BLI using an OctetRED96 instrument (ForteBio, Inc.) as previously described[8]. The biotinylated protein was loaded onto streptavidin optical biosensors and incubated with interacting protein. The results were processed and the association and dissociation plot and kinetic constants ($K_{on}$ and $K_{off}$) were obtained from ForteBio data analysis software. Equilibrium dissociation constants ($K_d$) were calculated by the ratio of $K_{off}$ to $K_{on}$.

### 2.19. In situ proximity ligation assay (PLA) assay

The *in situ* PLA was performed according to the manufacturer's instructions (Sigma−Aldrich). Cells were fixed in 3.7% paraformaldehyde for 20 min, permeabilized, and blocked before the addition of the primary antibody for immune-fluorescence analysis. The cells were then incubated with two primary antibodies derived from different species to recognize FXR and indicated proteins at 4 °C overnight. On the following day, cells were washed in Buffer A and incubated with secondary antibodies conjugated with oligonucleotides for 1 h at 37 °C. The ligation reaction was performed at 37 °C for 30 min, followed with amplification reaction at 37 °C in a darkened

humidified chamber. After washed by Buffer B, the samples were stained with DAPI and analyzed using a Zeiss 710 confocal microscope.

### 2.20. Statistical analysis

For all analysis in cell lines, the experiments were biologically repeated for three independent times. Results are presented as the mean ± standard error of mean (SEM). Statistical analysis of data was performed using GraphPad Prism (version 8.0). A two-tailed Student's *t*-test was applied for comparison of two groups and a one-way ANOVA with Tukey post hoc analysis was applied for comparison of multiple groups. *P* values below 0.05 were considered statistically significant.

## 3. Results

### 3.1. Loss of hepatic FXR underlies the compromised efficacies of FXR agonists in injured livers

We previously observed a gradual loss of hepatic FXR protein accompanied by the progressive development of fibrosis in fibrotic patients[8]. Here we verified whether such a reduction in FXR protein is conserved in diverse liver diseases. Murine liver injuries were induced by $CCl_4$ injection, BDL, and HFHC or MCD diet feeding. As expected, drastic decreases in hepatic FXR protein levels were observed in injured livers in all of these murine models, as shown by immunohistochemical (IHC) and Western blot analyses (Fig. 1A and B). Apoptosis and inflammation represent common pathological events across diverse liver diseases; thus, we tested whether apoptotic and inflammatory challenges would lead to a reduction in FXR protein level. Apoptosis was triggered by treatment of ActD/TNF$\alpha$, CHX/FasL, or TRAIL, and analyzed by CCK-8 assay and Annexin V-FITC/PI staining (Supporting Information Fig. S1A and S1B). Inflammation was induced by TNF$\alpha$ treatment and indicated by elevated cytokines (Fig. S1C). As expected, a gradual loss of FXR protein was observed in apoptotic and inflammatory HepG2 cells (Fig. 1C and Fig. S1D)[25]. It is reasonable to predict that decreased FXR level may compromise the hepatoprotective benefits of FXR agonists in injured livers. To this end, mice were injected with AAV *Fxr* shRNA to knock down hepatic FXR expression to mimic FXR loss in liver disease (Supporting Information Fig. S2A and S2B). These mice were then administered with $CCl_4$ and OCA (Fig. 1D). In mice injected with AAV Ctrl shRNA, OCA administration showed powerful hepatoprotective effects against $CCl_4$, as demonstrated by serum transaminase levels and histological analysis (Fig. 1E and F). Since $CCl_4$ treatment triggers the activation of hepatic stellate cells (HSCs), characterized as increased collagen deposition and elevated expression of pro-fibrotic genes, including *Acta2*, *Tgfb1*, *Col1a1*, and *Col1a2*. Results from Sirius red and Masson staining (Fig. 1F) and pro-fibrotic genes expression (Fig. S2C) demonstrated that OCA administration exhibited excellent effect in preventing HSC activation. Conversely, in mice injected with AAV *Fxr* shRNA, OCA administration was unable to transactivate FXR signals or protect the mice from $CCl_4$-induced acute liver injury and HSC activation (Fig. 1E and F, and Fig. S2B and S2C). Mice were injected with $CCl_4$ to induce overt loss of FXR (Fig. S2D) and then treated with OCA (Fig. 1G). As expected, therapeutic administration of OCA resulted in marginal hepatoprotection (Fig. 1H, I, Fig. S2E and S2F). Conversely, enforced expression of FXR by Ad-*Fxr* injection (Fig. 1J) not only enhanced FXR expression (Fig. S2G) but also restored the hepatoprotective effects of OCA (Fig. 1K, L, Fig. S2H and S2I), indicating that the FXR protein level is an important determinant for the efficacy of FXR agonists. Importantly, in line with our previously findings[8], enforced FXR overexpression *per se* was protective against $CCl_4$-induced liver injury, supporting an additional ligand-independent effects of FXR in combating apoptosis. These results suggest that the FXR protein level tends to decrease in conditions of diverse liver diseases, which compromises the hepatoprotective benefits of FXR agonists, and restoration of FXR protein level is important to strengthening both the canonical and noncanonical effects of FXR.

### 3.2. Cytoplasmic CHIP mediates FXR degradation upon apoptotic stimulation

We hypothesized that facilitated protein degradation by proteasomal or lysosomal activities may be involved in apoptotic HepG2 cells. Bafilomycin A1 (autophagy inhibitor) treatment resulted in little recovery of FXR loss. In contrast, MG132 (proteasome inhibitor) treatment resulted in an entire blockage of FXR loss (Fig. 2A), accompanied by the accumulation of ubiquitinated FXR in apoptotic HepG2 cells (Fig. 2B). This suggests that the increased ubiquitination targets FXR in the proteasome for degradation. We intended to identify the specific E3 ligase that mediates the ubiquitination and degradation of FXR. Potential E3 ligase of FXR was then searched in the UbiBrowser (obibrowser.ncpsb.org/)[26]. The data indicate that NEDD4, MDM2, ITCH, STUB1, UBE4B, BARD1 and SMURF1 might be involved in ubiquitin-mediated degradation of FXR (Supporting Information Fig. S3A). To explore which ligase serves as the E3 ligase for FXR during apoptosis, Co-IP assay was conducted to investigate the potential interactions. An enhanced association between FXR and NEDD4, ITCH, STUB1, BARD1, and SMURF1 was observed in apoptotic HepG2 cells (Fig. S3B). To further confirm which of these mediated FXR degradation, specific siRNAs targeting the above five candidates were transfected into HepG2 cells, which were then exposed to ActD/TNF$\alpha$. The results show that FXR degradation in apoptotic HepG2 cells was abolished by STUB1 siRNA transfection (Fig. S3C), indicating that STUB1 serves as the E3 ligase for FXR degradation upon apoptotic stimulation. CHIP (the carboxyl-terminus of Hsp70 interacting protein), encoded by STIP1 homology and U-Box containing protein 1 (STUB1), is a well-known E3 ubiquitin ligase. Additionally, recombinant GST-FXR was able to bind to CHIP in HepG2 lysates (Fig. 2C). The direct FXR−CHIP interaction was further validated using BLI assay (Fig. 2D). Next, we explored the binding domain involved in this interaction. CHIP contains an N-terminal tetratricopeptide repeat (TPR) domain, which allows for interaction with the C-terminus of Hsp70, and a C-terminal U-Box domain, which is responsible for E3 ubiquitination activity. FXR protein has a typical NR structure composed of modular domains, including the N-terminal ligand-independent transcriptional activation AF1 domain, DNA-binding domain (DBD), hinge region, and C-terminal ligand-binding domain containing a transcriptional activation function domain 2. Results show that the CHIP U-Box region was required for its interaction with FXR (Fig. 2E), whereas the FXR DBD domain

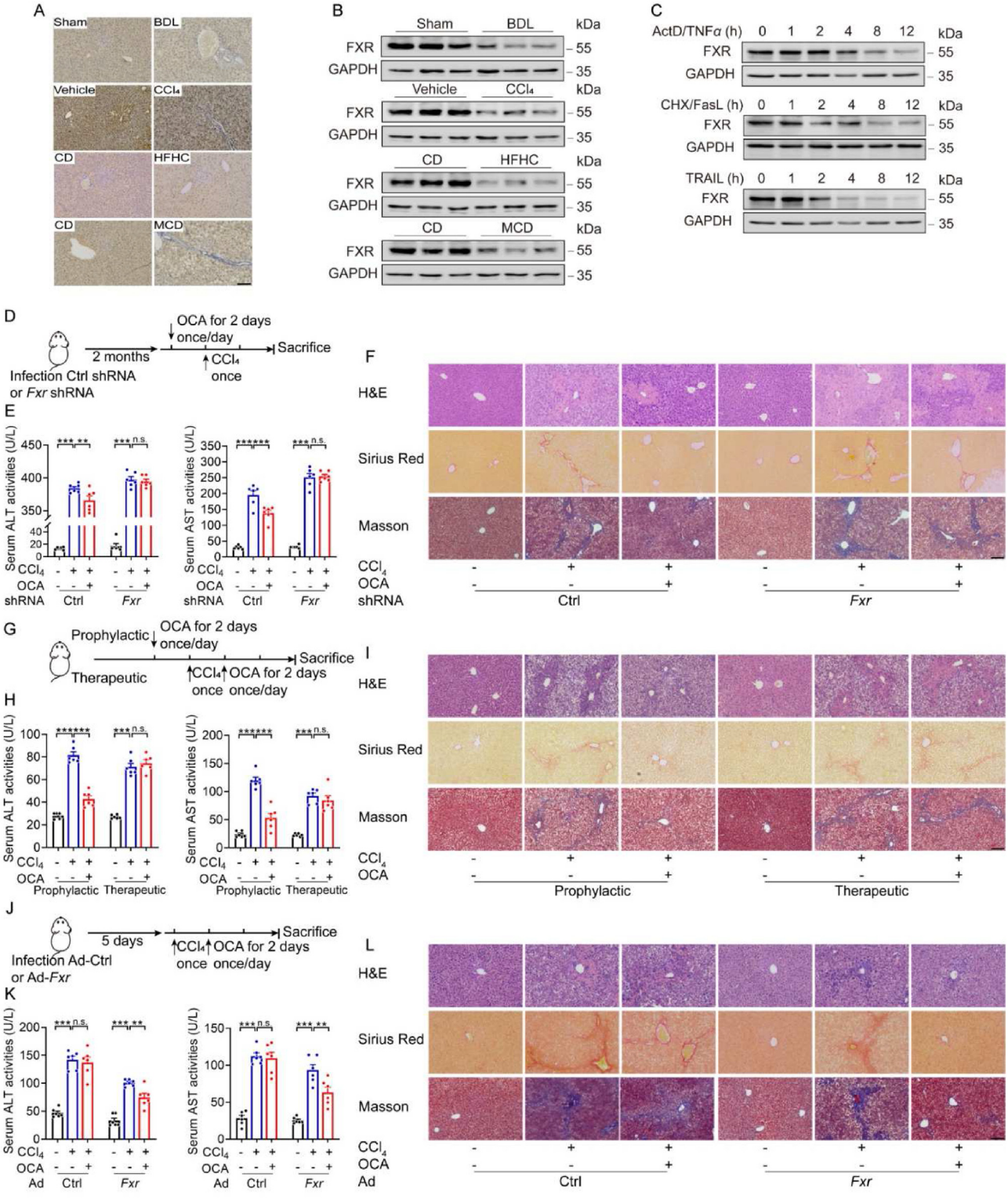


**Figure 1** Loss of hepatic FXR underlies compromised efficacies of FXR agonists in injured livers. (A, B) Reduced levels of FXR protein under various liver injuries, including BDL-induced cholestasis, $CCl_4$-induced acute liver injury, HFHC-and MCD diet-induced NASH by IHC (A) and Western blot (B). (C) FXR protein degradation in apoptotic HepG2 cells triggered by ActD/TNF$\alpha$, CHX/FasL, and TRAIL. (D−F) Attenuated hepatoprotective effects of OCA in FXR knock-down mice caused by specific AAV *Fxr* shRNA injection. (G−I) Attenuated hepatoprotective effects of OCA in FXR down-regulated mice caused by $CCl_4$ injury. (J−L) Restored hepatoprotective effect of OCA in $CCl_4$-injured mice with reinforced injection of Ad-*Fxr*. (D, G and J) Mouse experiment procedure schemes. (E, H and K) Serum ALT and AST levels. (F, I and L) Representative H&E, Sirius Red and Masson staining of liver sections. Scale bar, 100 μm. $n = 6$ biologically independent samples within these experiments. Results are mean ± SEM, $^{**}P < 0.01$, $^{***}P < 0.001$, and ns, statistically not significant, as assessed with ANOVA.

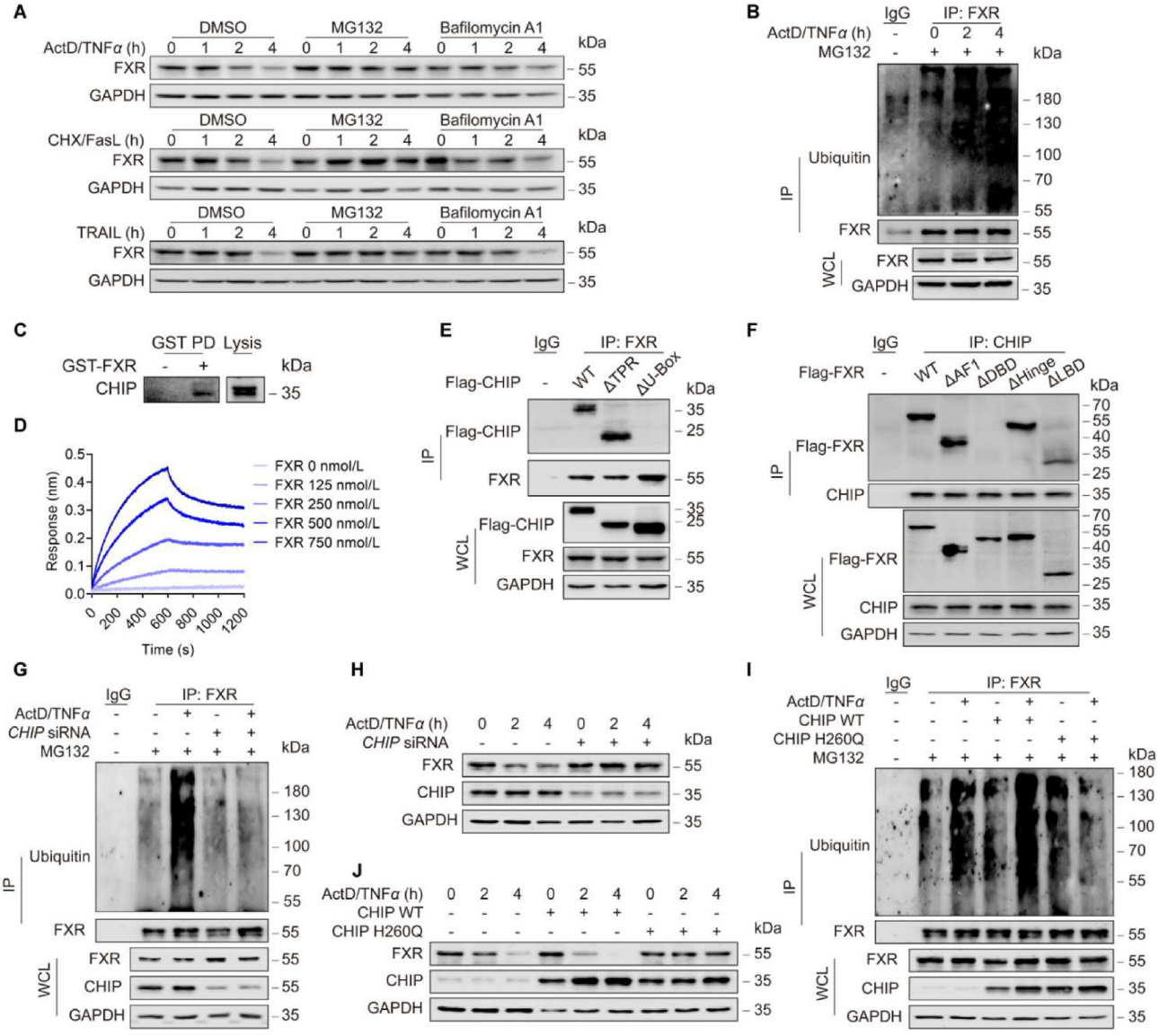


**Figure 2** Cytoplasmic CHIP mediates FXR degradation upon apoptotic stimulation. (A) Degradation of FXR protein in DRs-triggered apoptotic HepG2 cells were blocked by MG132, but not bafilomycin A1. (B) Ubiquitinated FXR accumulated in ActD/TNFα-treated HepG2 cells. (C, D) Interaction between CHIP and FXR by GST pull-down assay (C) and BLI assay (D). (E) FXR bound to the U-Box region of the CHIP protein. (F) CHIP bound to the DBD region of the FXR protein. (G, H) Knock-down of CHIP precluded the ubiquitination (G) and degradation (H) of FXR protein in ActD/TNFα-treated HepG2 cells. (I, J) CHIP WT but not CHIP H260Q, an E3 ligase activity mutant, overexpression enhanced poly-ubiquitination (I) and degradation (J).

was responsible for its interaction with CHIP (Fig. 2F). The role of CHIP in the ubiquitination and subsequent degradation of FXR was validated. As expected, suppressed FXR poly-ubiquitylation and degradation were observed following CHIP knockdown (Fig. 2G and H), whereas enhanced poly-ubiquitination and degradation were observed following CHIP overexpression (Fig. 2I and J). As with CHIP-mediated degradation of FXR, the E3 ligase activity of CHIP was required this regulation, as H260Q, an E3 ligase-defective mutant,[27] failed to induce ubiquitination or prevent degradation of FXR (Fig. 2I and J). Collectively, these data imply that CHIP is an E3 ligase of FXR that mediates ubiquitination and subsequent proteasomal degradation upon apoptotic stimulation.

### *3.3. Reduced KPNA3 interaction with FXR limits FXR nuclear import in apoptotic HepG2 cells*

CHIP is a cytosolic E3-ubiquitin ligase (Fig. S3D) that mediates the ubiquitination and degradation of various substrates within the cytoplasm[27]. FXR, a well-known NR member, is generally thought to function in the nucleus, suggesting that a nucleus-to-cytoplasm distribution of FXR occurs upon apoptotic stimulation (Supporting Information Fig. S3E). Furthermore, reduced nuclear localization and increased cytoplasmic retention of FXR were observed in the presence of MG132 (Fig. 3A and B). These results suggest that apoptotic challenge may favor the nucleus-to-cytoplasm distribution of FXR for degradation. This is supported

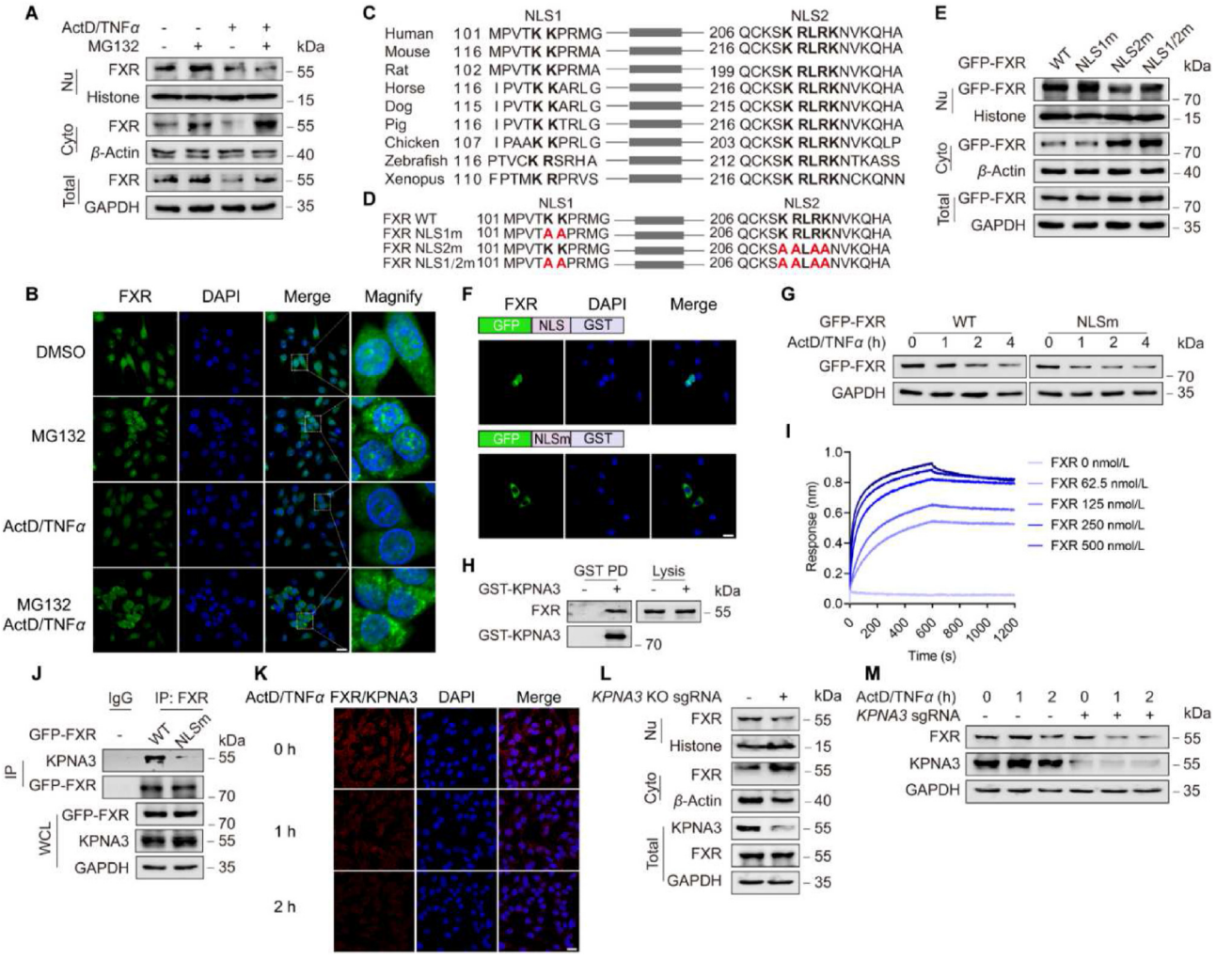


**Figure 3** Reduced KPNA3 interaction with FXR limits FXR nuclear import in apoptotic HepG2 cells. (A, B) Subcellular location of FXR in apoptotic HepG2 cells by Western blot (A) and immunofluorescence analysis (B). (C) Alignment of the FXR region containing predicted NLS sequences from various species. Predicted NLSs were indicated in boldface type. (D) Alignment of human FXR amino acids 101−120 and 201−220 around the predicted NLSs. Predicted NLSs were indicated in boldface type and the mutants were in red. (E) Mutation of predicted NLS2 but not predicted NLS1 of FXR caused its cytoplasmic accumulation. (F) Mutation of FXR NLS impaired its function in nuclear import as shown by cargo reporter. (G) Mutation of FXR NLS promoted its degradation upon apoptotic trigger. (H, I) Association between FXR and KPNA3 were detected by GST pull-down analysis (H) and BLI analysis (I). (J) Mutation of FXR NLS impaired the interaction between FXR and KPNA3 by Co-IP assay. (K) Reduced FXR-KPNA3 interaction in apoptotic HepG2 cells by PLA. (L) Knock-down of KPNA3 induced cytoplasmic accumulation of FXR. (M) KPNA3 knock-down accelerated FXR degradation triggered by ActD/TNFα. Scale bar, 20 μm.

by the fact that nuclear import by agonist restrict FXR degradation (Fig. S3F and S3G). Nucleocytoplasmic trafficking is an efficient mechanism for controlling the subcellular localization of proteins and may play an important role in orchestrating their functions and fates[28−30]. These results indicate that nucleocytoplasmic trafficking may be an important determinant of FXR degradation. Proteins with masses that exceeding ∼40 kDa (FXR, 55 kDa) shuttle between the nucleus and cytoplasm in active and signal-mediated pathways. Nuclear entry of a protein is determined by NLS, which typically contains clusters of positively charged basic amino acids of lysine (K) and arginine (R) separated by a spacer. Examination of the FXR amino acid sequence led us to identify two possible NLS sequences, which are highly conserved among mammalian, chicken, zebrafish, and xenopus (Fig. 3C). To test whether these putative sequences were FXR NLSs, amino acid substitutions (K or L to A) were introduced into these sequences (Fig. 3D). Results from cell fractionation assays show remarkably enhanced cytoplasmic localization of NLS2m compared with WT, suggesting that amino acids 210−214 (KRLRK) act as an NLS to mediate the cytoplasm-to-nucleus travel of FXR (Fig. 3E). To further validate whether this region is a functional NLS, we designed a cargo reporter in which GFP is expressed as a chimera with GST to increase its size so as to prevent passive diffusion to the nucleus[31], together with the FXR NLS fragment (amino acids 191−230), as shown in the schematic diagram (Fig. 3F). Results reveal that this NLS-cargo reporter was mainly localized in the nucleus, whereas amino acid substitutions (K or L to A) within the NLS caused a cytoplasmic retention of this cargo reporter (Fig. 3F). Importantly, mutation of this functional NLS sensitized FXR to apoptosis-triggered protein degradation (Fig. 3G). Taken

together, the FXR NLS motif, amino acids 210−214 (KRLRK), is important in mediating FXR cytoplasm-to-nucleus travel and subsequent FXR degradation. In the classical nuclear import pathway, the NLS motif is recognized by the adaptor protein importin $\alpha$, which is then tethered to importin $\beta$ and shuttles through the nuclear pore complex[32]. The importin $\alpha$ (also named as karyopherin subunit alpha, KPNA) family contains six isoforms; results from Co-IP assays showed that all these isoforms could interact with FXR. However, only the interaction between KPNA3 and FXR was attenuated upon apoptotic stimulation (Fig. S3H), suggesting that KPNA3 may be predominantly responsible for the nuclear localization of FXR. The interaction was validated by GST-pull down and BLI assay (Fig. 3H and I). Mutation of NLS impaired its association with KPNA3 (Fig. 3J), demonstrating that the FXR NLS is indeed recognized by KPNA3. More importantly, reduced association between FXR and KPNA3 in apoptotic cells was confirmed by *in situ* PLA analysis (Fig. 3K). These data suggest that KPNA3 recognizes the FXR NLS motif and directly interacts with FXR, which is compromised in apoptotic cells. Cell fractionation assays showed that KPNA3 knockdown promoted cytoplasmic retention and reduced nuclear accumulation of FXR protein (Fig. 3L). Importantly, KPNA3 knockdown also accelerated FXR degradation upon apoptotic trigger (Fig. 3M). These data suggest that KPNA3 acts as a functional importin for FXR. Collectively, we identified the FXR NLS motif, amino acids 210−214 (KRLRK), which is recognized by, and interacts with, KPNA3 to determine FXR cytoplasm-to-nucleus travel and prevent FXR degradation in the cytoplasm by CHIP.

### 3.4. *Enhanced CRM1/FXR interaction promotes nuclear export of FXR in apoptotic HepG2 cells*

Nucleocytoplasmic shuttling is also involved in nuclear export. Thus, we identified the signal in the FXR sequence and the translocator that mediates FXR export. Nuclear export of proteins is facilitated by nuclear export signal (NES), which is characterized by the presence of hydrophobic residues, such as leucine (L), and is typically sequenced as $LX_{2-3}LX_{2-3}LXL$ (X means any amino acid). We first analyzed the FXR amino acid sequence in search of possible NESs. Two sequences including "LQEPLLDVL" (amino acids 411−419) and "LLGRLTEL" (amino acids 437−444) within FXR fit the feature of classical NES, and these two motifs are evolutionarily conserved (Fig. 4A). We examined the nuclear export activities of these putative NESs by introducing mutations (L to A) and analyzed their subcellular localization (Fig. 4B). Mutation of either of the predicted NESs induced conspicuous nuclear accumulation of FXR (Fig. 4C). To further validate that these motifs are functional NESs, we constructed another cargo reporter by infusing the NES fragment (NES1: amino acids: 401−428; NES2: amino acids: 429−454) at the C-terminal of GST tag of above NLS-cargo (Fig. 4D). As expected, infusion of FXR NES fragments relocalized the NLS-cargo to the cytoplasm, whereas infusion of mutant FXR NES fragments did not (Fig. 4D). Furthermore, mutation of either NESs prevented FXR degradation upon apoptotic challenge (Fig. 4E), supporting that these two FXR NES motifs controlled the nucleus-to-cytoplasm travel and the degradation of FXR. We identified exportin, which is responsible for FXR nuclear export. Exportin chromosome region maintenance 1 (CRM1, also named exportin one or XPO1), the most extensively studied exportin, recognizes the NES of proteins and interacts with the RanGTP protein to form the target protein/CRM1/RanGTP complex to export target proteins out of the nucleus[33]. The $Ca^{2+}$-binding protein calreticulin (CRT) may participate in the nuclear export of several NRs.[34] Thus, we tested the possible role of CRM1 and CRT in the nuclear export of FXR. Co-IP assays revealed an association between FXR and CRM1 as well as CRT (Fig. 4F). Knockdown of CRM1, but not CRT, induced an increase in FXR nuclear localization (Fig. S3I and S3J), suggesting that CRM1 may mediate the nucleus-to-cytoplasm travel of FXR. Their association was further validated by GST-pull down and BLI assays (Fig. 4G and H). Mutation of lysine to alanine within the FXR NESs impaired its association with CRM1 (Fig. 4I). In addition, treatment with leptomycin B, which blocks the interaction between CRM1 and NES, induced the nuclear accumulation of FXR (Fig. 4J). These data collectively demonstrate that CRM1 recognizes FXR NESs, directly interact with FXR, and is responsible for its export out of the nucleus. Of interest, upon apoptotic stimulation, the interaction between CRM1 and FXR was enhanced (Fig. 4K and L), leading to enhanced nuclear export of FXR. Consistently, CRM1 knockdown prevented apoptosis-induced FXR degradation (Fig. 4M), supporting that CRM1 controls FXR nuclear export by recognizing its NES sequences.

### 3.5. *Acetylation of FXR controls its nucleocytoplasmic shuttling*

Our results show that FXR interacts with importin KPNA3 and exportin CRM1 to determine its nucleocytoplasmic shuttling and, thereafter, the protein degradation in the cytoplasm by CHIP. Apoptotic stress results in increased retention of FXR in the cytoplasm amenable to proteasomal degradation, *via* strengthening FXR/CRM1 interaction promoting nuclear export and concomitantly impaired FXR/KPNA3 interaction preventing nuclear import. We asked how this nucleocytoplasmic shuttling is tuned to adjust FXR function, and hypothesized that post-translational modification may be involved in this process. Protein sequence alignment around the NLS motif showed that K217 is evolutionarily conserved (Fig. 5A). Previous studies have demonstrated that K217 is the major acetylation site of FXR.[35] Conspicuous elevated acetylation upon apoptotic stimulation was observed in cells transfected with the FXR WT plasmid, but not in those transfected with the FXR K217R plasmid (Fig. 5B). Since acetylation neutralizes the positive charge of lysine residues and acetylation of lysine within NLS often influences NLS function and cellular localization[36], we investigated whether acetylation of K217, which is closed to FXR NLS, would influence its function. To this end, we mutated K217 to glutamine (K217Q) or arginine (K217R). In contrast to the nuclear localization of FXR NLS WT cargo, the acetylation mimic mutant K217Q cargo was mainly localized in the cytoplasm, indicating that acetylation of K217 may disrupt the FXR NLS motif (Fig. 5C). Epitope-tagged FXR WT, K217R, or K217Q mutant was expressed in HepG2 cells, and their subcellular distribution was analyzed. Consistent with the results from cargo reporter assays, K217R mutation led to constitutive nuclear localization (Fig. 5D). These results suggest that K217 acetylation impairs NLS function and FXR nuclear translocation. As expected, FXR with the K217Q mutation abolished its interaction with KPNA3, indicating that K217 acetylation impaired the recognition of NLS by KPNA3 (Fig. 5E). To eliminate the possible nonspecific effects derived from amino acid substitution, we synthesized biotinylated peptides around the FXR NLS motif (amino acids 191−230) containing either non-acetylated or acetylated K217 residues. Results from BLI assays

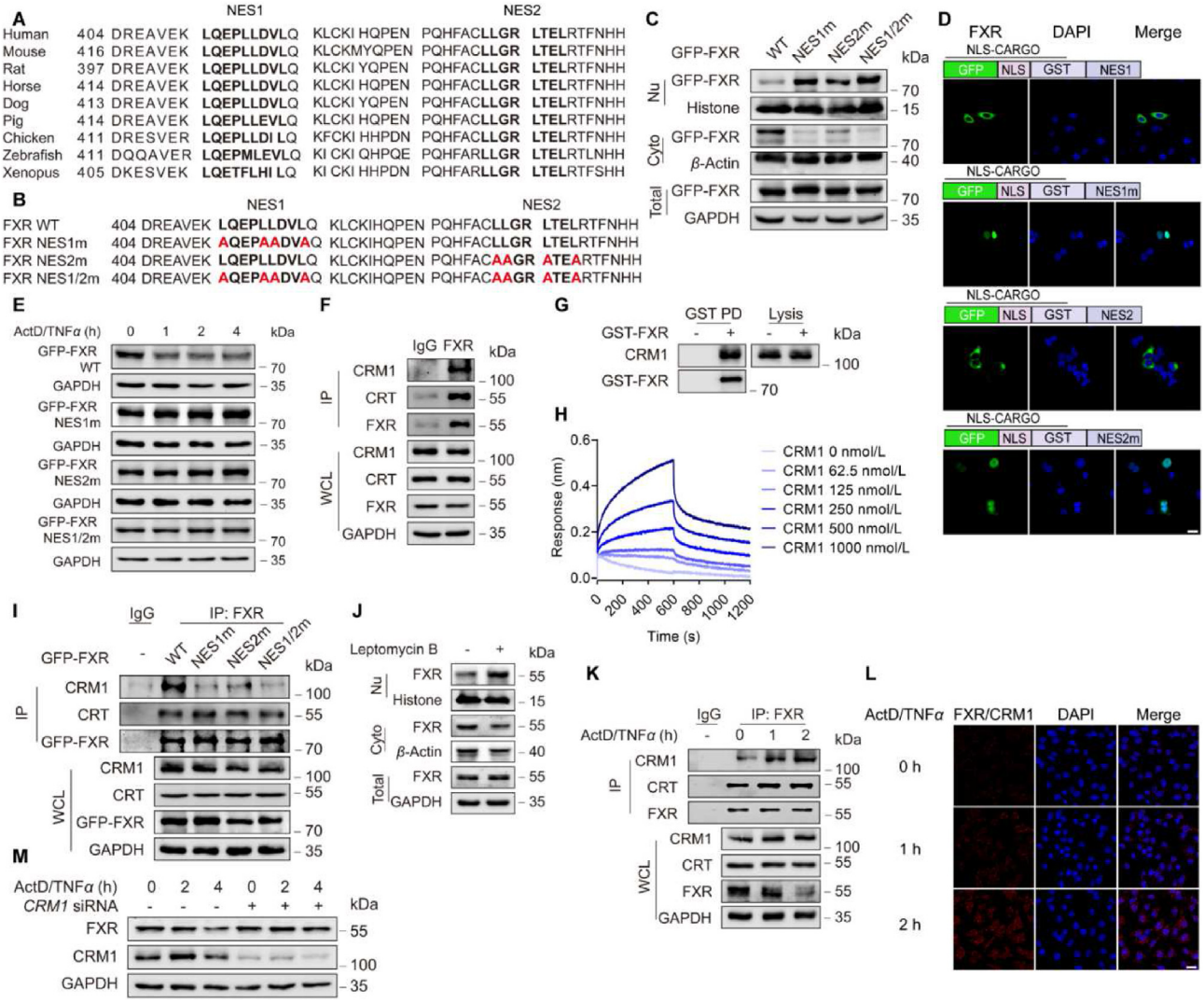


**Figure 4** Enhanced CRM1/FXR interaction promotes nuclear export of FXR in apoptotic HepG2 cells. (A) Alignment of the FXR region containing predicted NES sequences from various species. Predicted NESs were indicated in boldface type. (B) Alignment of human FXR amino acids 404−450 around the predicted NESs. Predicted NESs were indicated in boldface type and the mutants were in red. (C) Mutations of FXR NESs caused its nuclear retention. (D) Mutations of FXR NESs impaired their functions in nuclear export of NLS cargo reporter. (E) Mutations of FXR NESs prevented its degradation upon apoptotic trigger. (F−H) Association between FXR and CRM1 was detected by Co-IP analysis (F), GST pull-down analysis (G) and BLI analysis (H). (I) Mutations of FXR NESs impaired the interaction between FXR and CRM1. (J) Leptomycin B, a CRM1 inhibitor, prevented nuclear export of FXR protein. (K and L) Enhanced FXR-CRM1 interaction in apoptotic HepG2 cells by Co-IP assay (K) and PLA (L). (M) CRM1 knock-down by specific siRNA transfection prevented FXR degradation stimulated by ActD/TNFα. Scale bar, 20 μm.

showed that both K217-unacetylated and K217-acetylated peptides bound to KPNA3 at $K_d$ values of $1.74 \times 10^{-8}$ mol/L and $5.10 \times 10^{-8}$ mol/L, respectively (Fig. 5F). These results indicate that K217 acetylation impairs the affinity of FXR NLS to KPNA3, providing a reasonable explanation for the decreased FXR−KPNA3 interaction in apoptotic HepG2 cells. Upon apoptotic stimulation, a reduced association between CHIP and FXR K217R mutant and an enhanced association between CHIP and FXR K217Q mutant were observed, compared with FXR WT (Fig. 5E). Consistent results were obtained from the ubiquitination assay (Fig. 5G). As a further support, the acetylation-mimetic mutant was degraded much faster than FXR WT, whereas the acetylation-deficient mutant was degraded more slowly upon apoptotic trigger (Fig. 5H). Importantly, FXR acetylation increased promptly and gradually upon apoptotic stimulation (Fig. 5I), which was in line with the facilitated degradation of FXR. Collectively, these results support the notion that upon apoptotic stimulation, acetylation of FXR at K217 closed to NLS is significantly elevated, which represses FXR NLS−KPNA3 interaction and nuclear import, and thereafter facilitates CHIP-mediated degradation *via* the UPS.

We explored whether post-translational modification (PTM) also interfered with FXR-CRM1 interaction. Analysis of the amino acids within the NES motifs (amino acids 411−419 and 437−444) revealed an evolutionarily conserved residue threonine 442 (Supporting Information Fig. S4A), which has been reported

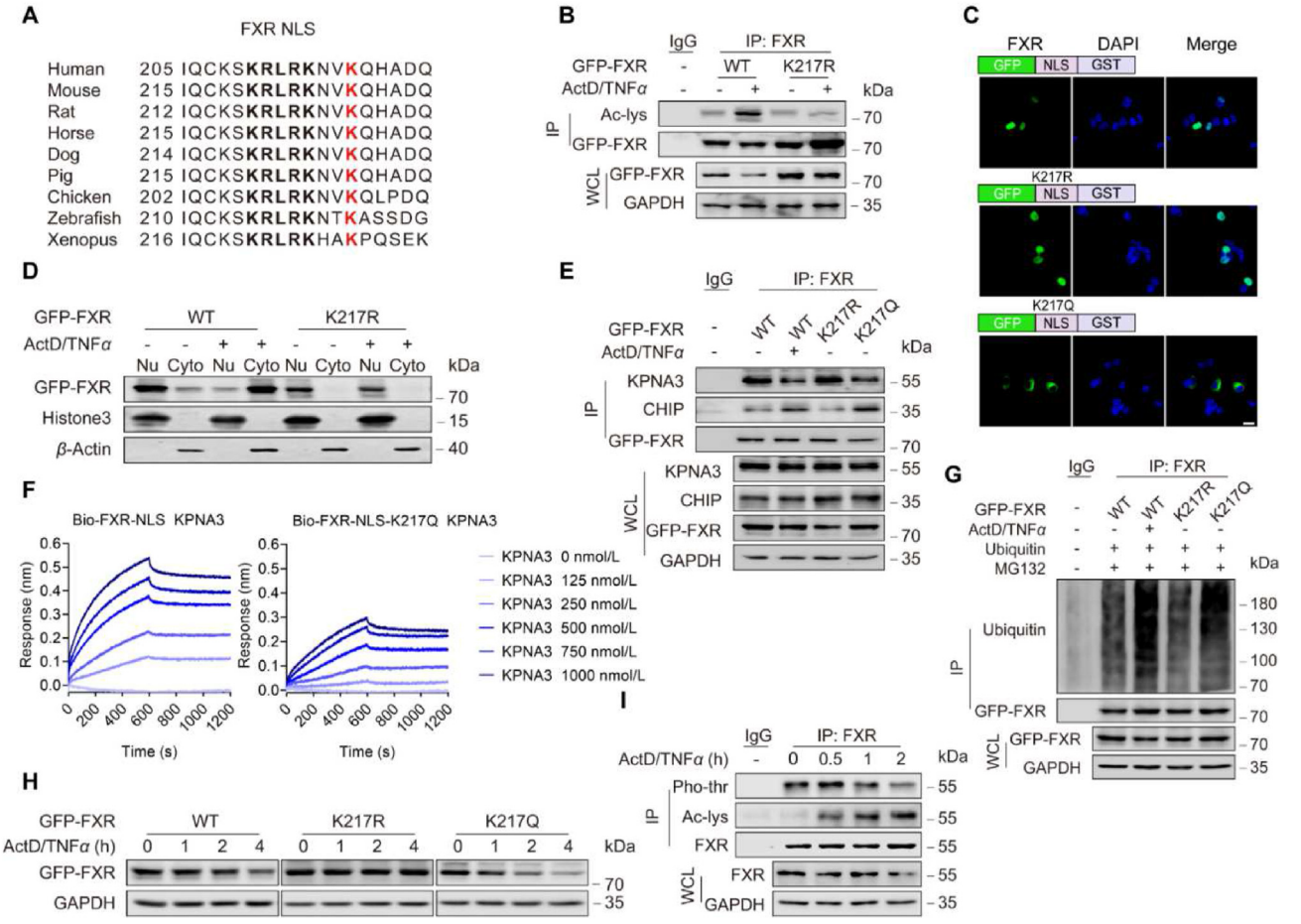


**Figure 5** FXR posttranslational modification controls its nucleocytoplasmic shuttling. (A) The lysine residue (K217 in human) closed to FXR NLS is evolutionarily conserved in vertebrates. Alignment of the FXR sequence surrounding K217 (human) from various species. The NLSs were indicated in boldface type and the lysine residues were in red. (B) Acetylation at FXR K217 increased in ActD/TNFα-treated HepG2 cells. (C) Subcellular distribution of FXR K217R-NLS cargo and FXR K217Q-NLS cargo compared with FXR WT-NLS cargo by fluorescence images. (D) Subcellular location of acetylation defective mutation K217R compared with FXR WT in ActD/TNFα-treated HepG2 cells by cell fractionation. (E) FXR K217 acetylation impaired FXR-KPNA3 interaction while promoted FXR-CHIP interaction by Co-IP analysis. (F) FXR K217 acetylation impaired the interaction between FXR NLS peptide and KPNA3 by BLI assay. (G) FXR K217 acetylation promoted its ubiquitination. (H) FXR K217 acetylation accelerated its degradation caused by ActD/TNFα. (I) FXR acetylation increased promptly and gradually upon apoptotic stimulation. Scale bar, 20 μm.

as a major phosphorylation site of FXR[37]. Mutagenesis was used to confirm that FXR phosphorylation at T442 was decreased by ActD/TNFα treatment (Fig. S4B). Thus, we supposed that FXR T442 phosphorylation impairs NES function and blocks its nuclear export. To this end, T to E (T442E) and T to A (T442A) replacements were used to generate a phosphorylation-mimic mutant and a phosphorylation-deficient mutant, respectively. Similar to the cargo infused with NES WT, the cargo infused with T442A NES motif mainly retained in the cytosol. In contrast, the cargo infused with T442E NES motif mainly localized in the nucleus (Fig. S4C). We next investigated whether phosphorylation of FXR at T442 is important for nucleus-to-cytoplasm trafficking of FXR. Compared with FXR WT, enhanced nuclear accumulation and reduced cytoplasmic localization were observed for the phosphorylation-mimic mutant T442E (Fig. S4D). Co-IP assays showed that the replacement of T442 by phosphorylation-mimetic amino acids disrupted the interaction between FXR and CRM1 (Fig. S4E). To provide a better understanding of how phosphorylation of FXR at T442 affected its recognition by CRM1, we performed BLI assays with biotinylated peptides containing NES motifs (amino acids 401−454) with either non-phosphorylated or phosphorylated T442 residues. T442-non-phosphorylated and T442-phosphorylated peptides bind to CRM1 at $K_d$ values of $9.01 \times 10^{-8}$ mol/L and $1.81 \times 10^{-7}$ mol/L, respectively (Fig. S4F). These data support the hypothesis that T442 phosphorylation leads to decreased recognition of FXR NESs by CRM1. We investigated the effect of T442 phosphorylation on FXR degradation induced by apoptosis. As expected, slower degradation was observed for ectopic expression of the phosphorylation-mimetic mutant (T442E) compared with WT (Fig. S4G).

Our results indicate that acetylation and phosphorylation of FXR function synergistically and culminate in increased cytoplasmic retention and the subsequent facilitated degradation. We asked whether and how the acetylation was coupled with phosphorylation. Of interest, upon apoptotic stimulation, changes in

FXR acetylation levels occurred earlier than the changes in phosphorylation levels (Fig. 5I). Acetylation can either positively or negatively regulate the phosphorylation of the same substrates[38,39], and *vice versa*[40,41]. Therefore, we were interested to investigate whether FXR acetylation and phosphorylation work independently or synergistically to modulate nucleocytoplasmic shuttling. Hence, we transfected WT, acetylation-mimicking K217Q mutant, or acetylation-resistant K217R mutant into HepG2 cells and analyzed their phosphorylation status. Results from Co-IP assays showed decreased phosphorylation modification of the K217Q mutant when compared with FXR WT (Fig. S4H). In contrast, no obvious difference in acetylation levels was observed between ectopically expressed FXR WT, T442E mutant, and T442A mutant (Fig. S4I). These results suggest that FXR acetylation may regulate subsequent phosphorylation but not *vice versa*. Taken together, our results indicate that acetylation may drive and orchestrate the process of nucleocytoplasmic shuttling and protein degradation of FXR, shedding light on the exploitation of FXR as a druggable target.

### *3.6. SIRT1 deacetylates FXR and governs its nucleocytoplasmic shuttling and degradation*

Our results suggest that acetylation is a driving factor in orchestrating FXR nucleocytoplasmic shuttling and protein degradation. Thus, we supposed that targeting acetylation may represent a promising strategy for strengthening FXR function. In agreement with a previous report, an interaction between P300 and FXR was readily detected (Fig. 6A). However, marginal alteration of this interaction was observed upon apoptotic stimulation (Fig. 6B). It has been well recognized that acetylation of substrate proteins is a dynamic process that can be catalytically reversed by specific deacetylases, including Sirtuin family (SIRT) and histone deacetylases. Stimulation of FXR acetylation by nicotinamide (NAM, an inhibitor of SIRT family) rather than by trichostatin A (TSA, an inhibitor of histone deacetylase I/II) suggests the involvement of SIRT family deacetylases (Supporting Information Fig. S5A). We then tested which SIRTs could specifically deacetylate FXR. Treatment with EX527, an inhibitor of SIRT1, yielded an effect in

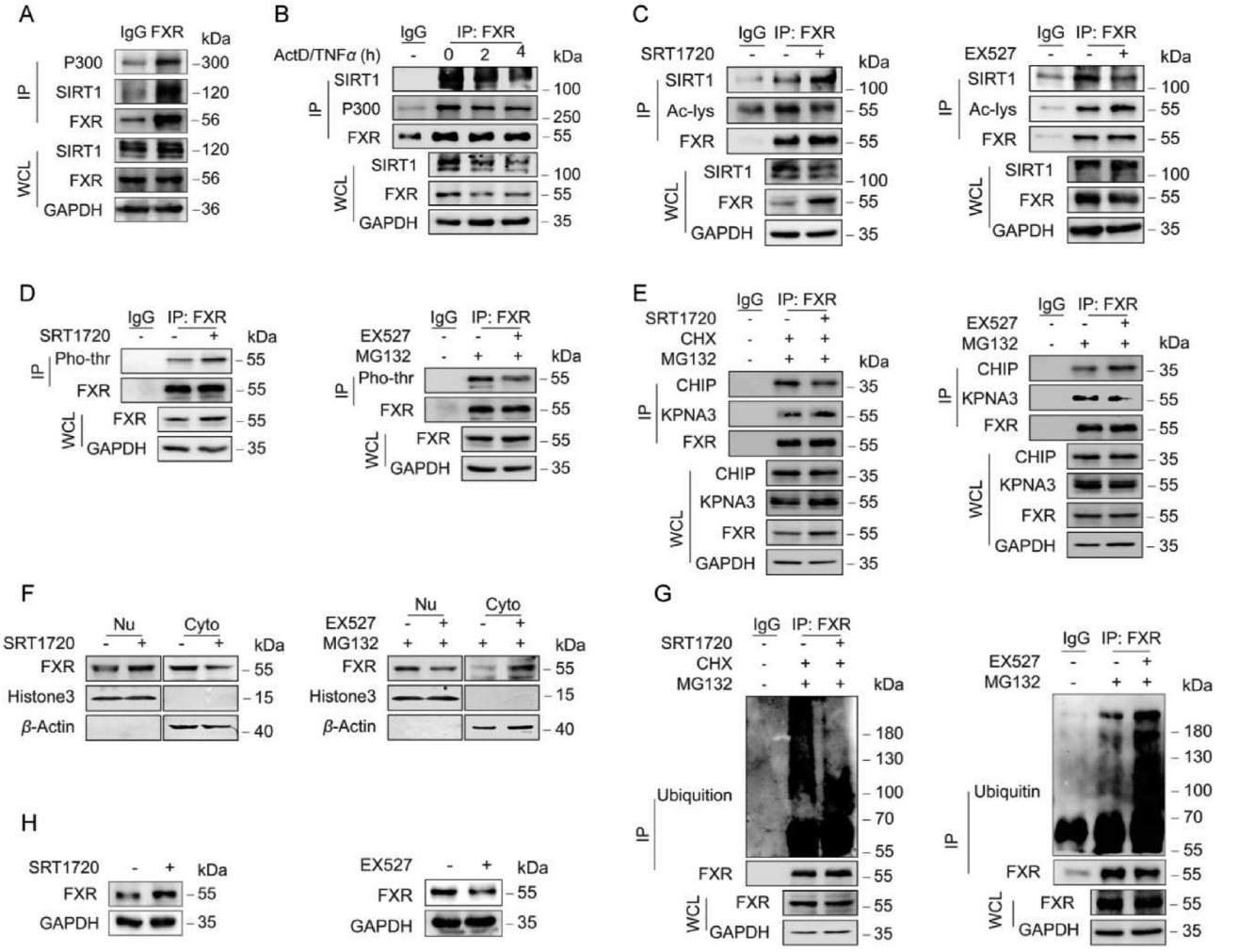


**Figure 6** SIRT1 deacetylates FXR and governs its phosphorylation, nuclear export, ubiquitination and degradation. (A) Association between P300/SIRT1 with FXR as detected by Co-IP analysis. (B) Reduced association between FXR and SIRT1 in ActD/TNFα-treated HepG2 cells by Co-IP analysis. (C) SIRT1 activation by SRT1720 promoted its association with FXR and inhibited FXR acetylation, and *vice versa.* (D) SRT1720 treatment enhanced FXR phosphorylation, and *vice versa.* (E) SRT1720 treatment promoted FXR−KPNA3 interaction while attenuated FXR−CHIP interaction, and *vice versa.* (F) SIRT1 activation by SRT1720 increased nuclear accumulation of FXR, and *vice versa.* (G) SIRT1 activation by SRT1720 decreased ubiquitination of FXR, and *vice versa.* (H) SIRT1 activation by SRT1720 stabilized the protein expression of FXR, and *vice versa*.

stimulating FXR acetylation similar to NAM (Fig. S5B), suggesting that SIRT1 controls the deacetylation of FXR. Results from Co-IP assay confirmed the association between FXR and SIRT1 (Fig. 6A), which is consistent with the results of a previous study[35]. Importantly, this association, as well as the SIRT1 protein expression, dramatically decreased upon apoptotic stimulation (Fig. 6B). In support of the role of SIRT1 in FXR acetylation, activation of SIRT1 by its activator SRT1720[42] promoted FXR−SIRT1 interaction and decreased FXR acetylation, whereas inhibition of SIRT1 by EX527 exhibited opposite effects (Fig. 6C). Genetic or chemical regulation of SIRT1 has marginal effects on the mRNA expression of FXR (Fig. S5C and S5D). In support of the acetylation-phosphorylation relay-mediated nucleocytoplasmic shuttling of FXR, SIRT1 activation or overexpression also resulted in enhanced FXR phosphorylation, enhanced FXR−KPNA3 interaction, increased nuclear accumulation, attenuated FXR−CHIP interaction, decreased ubiquitination, and decreased FXR degradation, whereas SIRT1 inhibition or knockdown exhibited the opposite effects (Fig. 6D−H, and Fig. S5E−S5J). Collectively, these results support that SIRT1 activation can be exploited as a strategy for retarding FXR degradation in the injured liver.

### *3.7. SIRT1 activators synergize with FXR agonists in combating acute and chronic liver injuries*

Above results show that SIRT1 activation may retard FXR degradation in HepG2 cells. Furthermore, this cascade of acetylation orchestrated nucleocytoplasmic shuttling and subsequent cytoplasmic degradation of FXR was further validated in AML12 cells, mouse normal hepatocytes (Supporting Information Fig. S6). We supposed that SIRT1 activation may synergize with FXR agonism in combating liver diseases. To this end, two murine liver injury models were used to determine the potential synergistic effects of SIRT1 activators and FXR agonists. Before $CCl_4$ injection, mice were injected with SRT1720, and 24 h after $CCl_4$ injection, mice were treated with OCA (Fig. 7A). Results from Co-IP assay confirm the enhanced acetylation and decreased phosphorylation of FXR in $CCl_4$-treated mice. What's more, FXR protein expression and transcriptional activity were dramatically suppressed upon $CCl_4$ injection, whereas SRT1720 treatment largely restored all of these changes (Fig. 7B−D). Serum levels of ALT and AST were dramatically reduced in mice co-treated with SRT1720 and OCA, but not in those treated with either one (Fig. 7E). Histological analysis demonstrated that co-treatment with SRT1720 and OCA attenuated hepatocellular injury and reduced extracellular matrix accumulation (Fig. 7F). Results from the mRNA expression analysis of pro-fibrotic genes provide further evidence for the powerful effect in preventing HSC activation of this combination (Fig. 7G).

The effects of this combination were validated in a murine model of NASH. Mice were fed with an HFHC diet for 16 consecutive weeks and treated with SRT1720 and OCA from 12th week and 13th week, respectively (Fig. 8A). As expected, SRT1720 treatment restored the FXR acetylation−phosphorylation balance, protein expression, and transcriptional activity (Fig. 8B−D). Results from serum aminotransferases and histological analysis demonstrated that SRT1720 treatment significantly synergized with OCA in protecting mice from NASH. Besides, in consistent with the results of H&E staining of liver sections, TG and TC levels in serum and livers further demonstrated the synergistic effect of SRT1720 and OCA in alleviating steatosis. Furthermore, mRNA levels of pro-fibrotic genes demonstrated that SRT1720 treatment significantly synergized with OCA in preventing HSC activation (Fig. 8E−I). Since both SIRT1 and FXR were identified as important targets in HSCs to inhibit its activation[43,44], we further evaluated the effect of combined SIRT1 activator and FXR agonist in HSC activation. Results show that in activated HSCs, SIRT1 activation slightly inhibits HSC activation, while FXR agonism exerts marginal effect. Pleasantly, combined SIRT1 activator and FXR agonist showed significant improved efficacy in inhibiting HSC activation (Supporting Information Fig. S7). Taken together, results from both acute and chronic liver injury models support the notion that SRIT1 activation is a promising strategy to strengthen the pharmacological benefits of FXR agonists.

## 4. Discussion

The discovery of FXR and its multiple functions has led to the investigation of FXR agonists as promising therapies for various liver diseases. However, the development of FXR ligands as drugs for liver diseases, particularly for NASH, has encountered difficulties because of their limited clinical benefits. We previously demonstrated that prophylactic but not therapeutic OCA administration impedes hepatic stellate cells activation and fibrosis development[10]. Notably, the FXR protein level in hepatocytes was found to gradually decrease with the development of fibrosis[45], but without a clear mechanism. Here, we uncovered an unexpected mechanism by which acetylation drives and orchestrates the nucleocytoplasmic shuttling and subsequent protein degradation of FXR in the cytoplasm by CHIP, shedding light on the precise regulatory dynamics of FXR. Based on these findings, we further validated that combination of SIRT1 activator and FXR agonists functions synergistically in combating liver injury, particularly NASH. Our findings may pave the way for the better exploitation of FXR as a target for many kinds of liver diseases.

NRs ligands operate *via* an "occupancy-driven" paradigm, where pharmacologically relevant inhibition or activation is often only achieved with high target engagement/occupancy. Thus, sufficient protein expression of NRs is essential for the pharmacological effects of NR ligands. In support of this notion, 17$\beta$-estradiol was demonstrated to be incapable of exerting significant neuroprotection in older rats as it does in young and middle-aged rats due to increased degradation and significant decrease in hippocampal ER$\alpha$ protein, another NR member, in older rats[46]. In the present study, we demonstrated that the hepatoprotective effects of OCA were compromised and/or abolished under conditions of FXR loss. Notably, a drastic decrease in hepatic FXR protein level was observed in NASH, primary biliary cirrhosis and fibrosis patients[8,15,16], as well as in animals suffered from various acute or chronic liver diseases. In $CCl_4$-injuried mice, therapeutic administration of OCA exerted marginal benefits in improving liver function, and Ad-*Fxr* injection restored hepatic FXR protein expression. These results provide direct evidence that reduced hepatic FXR protein levels in various liver diseases is the chief culprit for the limited clinical benefits of FXR agonists; thus, an innovative strategy to restore FXR protein level is of paramount importance to enhance the clinical benefits of FXR agonists, given that the mechanism of decreased FXR levels in injured liver is being clarified.

NRs mainly localize and function in the nuclear compartment. In addition to function fulfillment, protein degradation either by

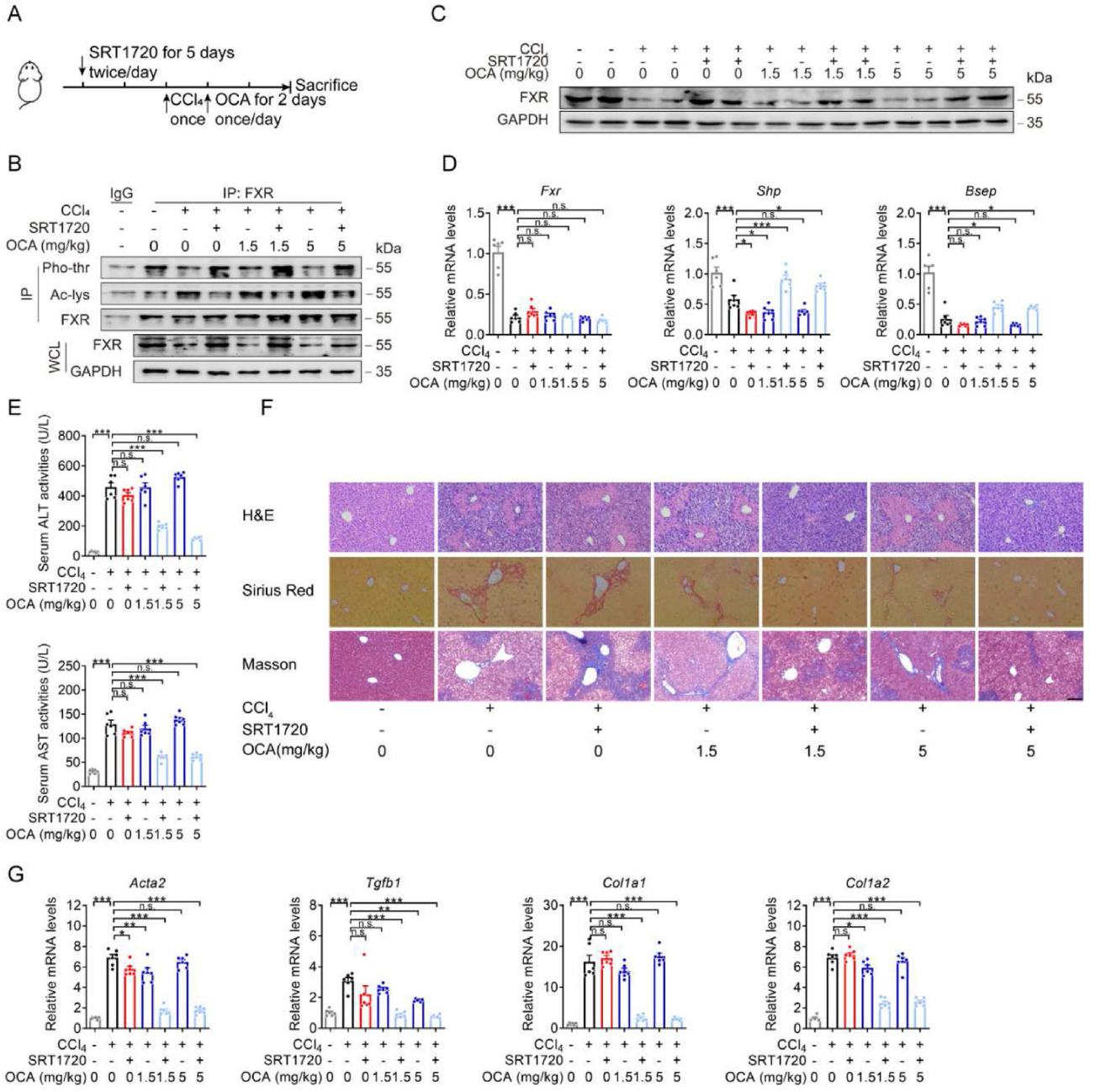


**Figure 7** SIRT1 activation synergizes with FXR agonism in combating acute liver injury *via* retarding FXR degradation. (A) Mouse experiment procedure schemes. (B) PTMs of hepatic FXR by IP analysis. (C) Protein levels of hepatic FXR by Western blot analysis. (D) Hepatic mRNA expression of *Fxr*, *Shp*, and *Bsep* relative to *Gapdh*. (E) Serum ALT and AST levels. (F) Representative H&E, Sirius Red and Masson staining of liver sections. (G) Hepatic mRNA expression of *Acta2*, *Tgfb1*, *Col1a1*, and *Col1a2* relative to *Gapdh*. $n = 6$ biologically independent samples within these experiments. Scale bar, 100 μm. Results are mean ± SEM, $^{*}P < 0.05$, $^{**}P < 0.01$, $^{***}P < 0.001$, and *ns*, statistically not significant, as assessed with ANOVA.

the UPS or autophagy is conducted based on compartmentalization[19]. A previous study demonstrated that 26S proteasomes, the core component of the UPS, are predominantly found in the nucleus, which is one of the compartments for protein degradation[47,48]. However, a latter study found that nuclear-localized proteasomes have drastically reduced peptidase activity compared with cytosolic proteasomes, suggesting that the cytosol is the prominent compartment for the degradation of intracellular proteins, including thousands of nuclear proteins[21]. In contrast to that of aboriginal proteins, cytosolic degradation of nuclear proteins poses significant topological problems. Thus, re-localization is required for the degradation of these proteins. However, the conserved mechanism for re-localization and cytoplasmic degradation of NRs and TFs remains unclear. In this study, taking FXR as a typical example, we revealed an unexpected mechanism that the cascades of PTMs are coupled with nucleocytoplasmic shuttling and subsequent cytoplasmic degradation, which may provide a universal mechanism for understanding the precise regulatory

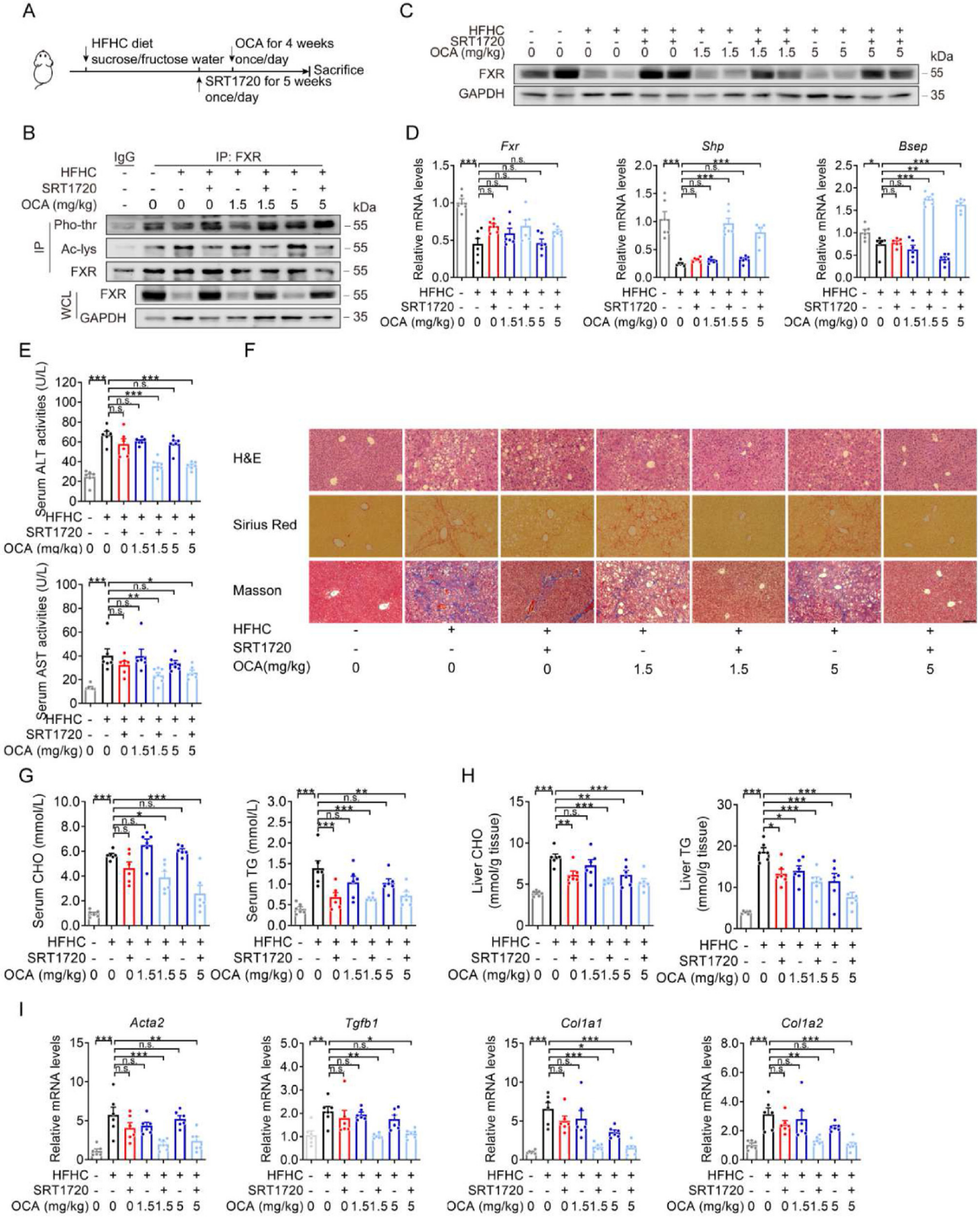


**Figure 8** SIRT1 activation synergizes with FXR agonism in combating NASH *via* retarding FXR degradation. (A) Mouse experiment procedure schemes. (B) PTMs of hepatic FXR by IP analysis. (C) Protein levels of hepatic FXR by Western blot analysis. (D) Hepatic mRNA expression of *Fxr*, *Shp*, and *Bsep* relative to *Gapdh*. (E) Serum ALT and AST levels. (F) Representative H&E, Sirius Red and Masson staining of liver sections. (G, H) TG and TC levels in serum (G) and livers (H). (I) Hepatic mRNA expression of *Acta2*, *Tgfb1*, *Col1a1*, and *Col1a2* relative to *Gapdh*. $n = 6$ biologically independent samples within these experiments. Scale bar, 100 μm. Results are mean ± SEM, $^{*}P < 0.05$, $^{**}P < 0.01$, $^{***}P < 0.001$, and ns, statistically not significant, as assessed with ANOVA.

loop of protein compartmentalization, function, and degradation. NRs and TFs, despite being traditionally localized in the nucleus, can traffic between the cytoplasm and nucleus[49]. Additionally, multiple cytoplasmic functions of several NRs and TFs have been uncovered.[50,51]. More recently, we demonstrated a cytoplasmic function against hepatocellular apoptosis of FXR[8], indicating that nucleocytoplasmic shuttling is an important feature of FXR, albeit with an unclear mechanism. Here, we found that the nucleocytoplasmic shuttling of FXR depends on its interaction with the importin KPNA3 and exportin CRM1. The association between FXR and KPNA3 was reduced, but that between FXR and CRM1 increase, upon apoptotic stimulation, culminating in excessive retention of FXR in the cytoplasm, where FXR is subjected to CHIP-mediated proteasomal degradation.

PTMs are crucial for the rapid adaption to cellular stress[52], and NLSs/NESs are usually regulated by PTMs to shuttle substrates. Acetylation of lysine(s) within the NLS motifs of S phase kinase-associated protein 2[36], phosphofructokinase-2/fructose-2,6-bisphosphatase 3[53] and γ-interferon-inducible protein 16[54] impairs their activities and accumulates these proteins in the cytoplasm. *O*-GlcNAcylation of serine/arginine-rich protein kinase two at NLS triggers its binding with importin and nuclear translocation[55]. Protein sequence alignment around the FXR NLS motif showed a conserved acetylation site at lysine 217. Genetic and peptide-level studies have demonstrated that K217 acetylation disrupted its recognition by KPNA3. Likewise, genetic and peptide-level studies demonstrated that T442 phosphorylation disrupts FXR recognition by CRM1. Upon apoptotic stimulation, FXR acetylation at K217 and phosphorylation at T442 dramatically increased and decreased, respectively. In addition to its regulation of transcriptional activity, a previous study has observed a positive correlation between FXR nuclear location and its phosphorylation at Y67 and T442[37], but without a clear mechanism. In the present study, we provided strong evidence that FXR T442 phosphorylation inhibits the activities of newly identified NESs and prevents their recognition by CRM1, precluding its nuclear export. In apoptotic cells, FXR phosphorylation is decreased, which results in enhanced nuclear-to-cytoplasm travel and cytoplasmic accumulation. FXR is acetylated by P300 and deacetylated by SIRT1, and K217 in the hinge region is the major acetylation site[35,56]. Importantly, we observed a crosstalk between PTMs of that acetylation in the cytoplasm may negatively regulate FXR phosphorylation in the nucleus. The possible mechanism for the control of phosphorylation by acetylation may lie in the spatial availability of FXR to specific phosphatases, which requires further investigation.

Our finding that acetylation is a driving factor in controlling the nucleocytoplasmic shuttling and subsequent protein degradation of FXR prompted us to test the potential synergistic effects of targeting the process of acetylation together with FXR agonists. In support of our hypothesis, enhanced FXR acetylation and reduced FXR protein expression caused by reduced SIRT1 expression have been observed in ANIT-induced cholestasis[57], cadmium chloride-induced NAFLD[58], and acetaminophen-induced liver injury[59]. SIRT1 activation partially alleviates cholestatic liver diseases by rescuing hepatic FXR hyperacetylation[60]. Naiara Beraza et al. [61,62] also reported that SIRT1 controls liver regeneration and cholestatic liver disease by modulating FXR. The pivotal roles of SIRT1 in NAFLD and fibrosis have been reported. The expression levels of SIRT1 were down-regulated in fibrotic livers as well as activated HSCs. Inhibition of hepatic SIRT1 by E3 ligase Grail promotes hepatic steatosis and development of NAFLD[63]. Loss of SIRT1 in HSCs promote the activation and trans-differentiation of HSCs into myofibroblasts, and then fibrosis[43,44]. Various natural and synthetic activators of SIRT1 have shown benefits in delaying aging, inhibiting inflammation, attenuating oxidative stress, precluding apoptosis and liver fibrosis. Some of these activators have been evaluated in various clinical trials in recent years[64]. SIRT1 exerts its multiple functions *via* its histone and non-histone deacetylase activities on various protein substrates, including various TFs (P65, P53, FoxO family, PGC1α, PPARγ, etc.). The deacetylation of these TFs by SIRT1 mildly promotes their transcriptional activation, and serves as a prerequisite for transcriptional activation by activators and/or agonists. However, SIRT1 activators *per se* are insufficient for combating pathological processes. Hence, SIRT1 activation may be necessary but not sufficient for transcriptional activation and function fulfillment of these TFs.

This study demonstrates that acetylation plays important roles in the hepatoprotective effects of FXR. De-acetylation improves the efficacy of FXR against acute and chronic liver diseases by restoring its protein expression in hepatocytes. In addition to acetylation, other PTMs also play pivotal roles in hepatoprotection effects of FXR. Previous study demonstrated that SUMOylation of FXR gradually elevated during activation of HSCs[10]. This study suggests that SUMOylation may largely contribute to the hepatoprotection effect of FXR against liver fibrosis by regulating its transcriptional activity.

Taken together, in this study, we provided the first line of evidence of that SIRT1 activators in combination with FXR agonists represent a promising therapeutic strategy against various liver diseases. The results obtained from this study may encourage future research to test the combination of SIRT1 activators and activators/agonists of TFs in diverse pathological settings.

## 5. Conclusions

We demonstrated in this study that SIRT1 activation synergizes with FXR agonism for hepatoprotection *via* governing nucleocytoplasmic shuttling and degradation of FXR. Acetylation initiates and orchestrates FXR nucleocytoplasmic shuttling and thereafter cytoplasmic degradation by CHIP in conditions of liver injury, which represents the major culprit for the limited therapeutic efficacy of FXR agonists in the clinic. Upon apoptotic stimulation, enhanced FXR acetylation at K217 closed to the NLS blocks its recognition by importin KPNA3, preventing the nuclear import of FXR protein. Concomitantly, reduced phosphorylation at T442 within NESs promotes its recognition by exportin CRM1, and thereby facilitating the nuclear export of FXR to the cytosol. Upon apoptotic and inflammatory stress, the enhanced acetylation governing nucleocytoplasmic shuttling of FXR results in its excessive cytoplasmic retention and degradation by CHIP. SIRT1 activators that reduce FXR acetylation reverse this process and synergize with FXR agonists in combating liver injury. Our findings reveal an important mechanism connecting PTMs to spatial distribution and thereby protein degradation process of FXR. We provided an innovative strategy as combining SIRT1 activator and FXR agonist with improved hepatoprotective benefits for liver diseases.

## Acknowledgments

This research is supported by the National Natural Science Foundation of China (grants 81720108032 and 81930109 to

Haiping Hao, 82073926 to Hong Wang, and 82073928 to Guangji Wang); the National Key Research and Development Programme of China (2021YFA1301300 to Haiping Hao); Leading Technology Foundation Research Project of Jiangsu Province (grant BK20192005 to Guangji Wang, China); the Project Program of State Key Laboratory of Natural Medicines (China Pharmaceutical University, SKLNMZZ202202 to Haiping Hao); and Sanming Project of Medicine in Shenzhen (SZSM201801060 to Guangji Wang, China).

## Author contributions

Shuang Cui, Huijian Hu, and Ming Cui designed and performed the experiments. An Chen, Xiaojie Pan, and Pengfei Zhang participated in performing the experiments. Shuang Cui, Huijian Hu, Hong Wang, and Haiping Hao analyzed the data. Hong Wang and Haiping Hao wrote and revised the manuscript. Guangji Wang participated in proofreading this manuscript. Hong Wang and Haiping Hao conceived and supervised the entire project.

## Conflicts of interest

The authors declare no conflicts of interests.

## Appendix A. Supporting information

Supporting data to this article can be found online at https://doi.org/10.1016/j.apsb.2022.08.019.

## References

1. Sanyal AJ. Past, present and future perspectives in nonalcoholic fatty liver disease. *Nat Rev Gastroenterol Hepatol* 2019;**16**:377−86.
2. Li TG, Chiang JYL. Bile acid-based therapies for non-alcoholic steatohepatitis and alcoholic liver disease. *Hepatobiliary Surg Nutr* 2020;**9**:152−69.
3. Cazanave SC, Warren AD, Pacula M, Touti F, Zagorska A, Gural N, et al. Peptide-based urinary monitoring of fibrotic nonalcoholic steatohepatitis by mass-barcoded activity-based sensors. *Sci Transl Med* 2021;**13**:eabe8939.
4. Clifford BL, Sedgeman LR, Williams KJ, Morand P, Cheng A, Jarrett KE, et al. FXR activation protects against NAFLD *via* bile-acid-dependent reductions in lipid absorption. *Cell Metabol* 2021;**33**:1671−16784.e4.
5. Collins SL, Patterson AD. The gut microbiome: an orchestrator of xenobiotic metabolism. *Acta Pharm Sin B* 2020;**10**:19−32.
6. Hao HP, Cao LJ, Jiang CT, Che Y, Zhang SY, Takahashi S, et al. Farnesoid X receptor regulation of the NLRP3 inflammasome underlies cholestasis-associated sepsis. *Cell Metabol* 2017;**25**:856−67.e5.
7. Wang YD, Chen WD, Wang M, Yu D, Forman BM, Huang W. Farnesoid X receptor antagonizes nuclear factor kappaB in hepatic inflammatory response. *Hepatology* 2008;**48**:1632−43.
8. Wang H, Ge CL, Zhou JY, Guo YT, Cui S, Huang NN, et al. Non-canonical farnesoid X receptor signaling inhibits apoptosis and impedes liver fibrosis. *EBioMedicine* 2018;**37**:322−33.
9. Seok S, Fu T, Choi SE, Li Y, Zhu R, Kumar S, et al. Transcriptional regulation of autophagy by an FXR−CREB axis. *Nature* 2014;**516**:108−11.
10. Zhou JY, Cui S, He QX, Guo YT, Pan XJ, Zhang PF, et al. SUMOylation inhibitors synergize with FXR agonists in combating liver fibrosis. *Nat Commun* 2020;**11**:240.
11. Sun LL, Pang YY, Wang XM, Wu Q, Liu HY, Liu B, et al. Ablation of gut microbiota alleviates obesity-induced hepatic steatosis and glucose intolerance by modulating bile acid metabolism in hamsters. *Acta Pharm Sin B* 2019;**9**:702−10.
12. Wang H, He QX, Wang GJ, Xu XW, Hao HP. FXR modulators for enterohepatic and metabolic diseases. *Expert Opin Ther Pat* 2018;**28**:765−82.
13. Younossi ZM, Ratziu V, Loomba R, Rinella M, Anstee QM, Goodman Z, et al. Obeticholic acid for the treatment of non-alcoholic steatohepatitis: interim analysis from a multicentre, randomised, placebo-controlled phase 3 trial. *Lancet* 2019;**394**:2184−96.
14. Eslam M, Alvani R, Shiha G. Obeticholic acid: towards first approval for NASH. *Lancet* 2019;**394**:2131−3.
15. Nobili V, Alisi A, Mosca A, Della Corte C, Veraldi S, De Vito R, et al. Hepatic farnesoid X receptor protein level and circulating fibroblast growth factor 19 concentration in children with NAFLD. *Liver Int* 2018;**38**:342−9.
16. Byun S, Kim DH, Ryerson D, Kim YC, Sun H, Kong B, et al. Post-prandial FGF19-induced phosphorylation by Src is critical for FXR function in bile acid homeostasis. *Nat Commun* 2018;**9**:2590.
17. Thul PJ, Akesson L, Wiking M, Mahdessian D, Geladaki A, Ait Blal H, et al. A subcellular map of the human proteome. *Science* 2017;**356**:eaal3321.
18. Orre LM, Vesterlund M, Pan YB, Arslan T, Zhu YF, Fernandez Woodbridge A, et al. SubCellBarCode: proteome-wide mapping ofprotein localization and relocalization. *Mol Cell* 2019;**73**:166−82.e7.
19. Pohl C, Dikic I. Cellular quality control by the ubiquitin-proteasome system and autophagy. *Science* 2019;**366**:818−22.
20. Lv SD, Song Q, Chen G, Cheng ED, Chen W, Ryan ColeWu Z, et al. Regulation and targeting of androgen receptor nuclear localization in castration-resistant prostate cancer. *J Clin Invest* 2021;**131**:e141335.
21. Dang FW, Chen L, Madura K. Catalytically active proteasomes function predominantly in the cytosol. *J Biol Chem* 2016;**291**:18765−77.
22. Metcalf MG, Higuchi-Sanabria R, Garcia G, Tsui CK, Dillin A. Beyond the cell factory: homeostatic regulation of and by the UPR(ER). *Sci Adv* 2020;**6**:eabb9614.
23. Cui S, Pan XJ, Ge CL, Guo YT, Zhang PF, Yan TT, et al. Silybin alleviates hepatic lipid accumulation in methionine−choline deficient diet-induced nonalcoholic fatty liver disease in mice *via* peroxisome proliferator-activated receptor alpha. *Chin J Nat Med* 2021;**19**:401−11.
24. Wang H, Yan TT, Xie Y, Zhao M, Che Y, Zhang J, et al. Mechanism-based inhibitory and peroxisome proliferator-activated receptor alpha-dependent modulating effects of silybin on principal hepatic drug-metabolizing enzymes. *Drug Metab Dispos* 2015;**43**:444−54.
25. Xu XW, Zhu Y, Song JZ, Zou GQ, Zhao Z, Zheng QL, et al. Selective photoaffinity probe for monitoring farnesoid X receptor expression in cultured cells. *Anal Chem* 2022;**94**:10722−9.
26. Li Y, Xie P, Lu L, Wang J, Diao LH, Liu ZY, et al. An integrated bioinformatics platform for investigating the human E3 ubiquitin ligase−substrate interaction network. *Nat Commun* 2017;**8**:347.
27. Qian SB, McDonough H, Boellmann F, Cyr DM, Patterson C. CHIP-mediated stress recovery by sequential ubiquitination of substrates and Hsp70. *Nature* 2006;**440**:551−5.
28. Wyant GA, Abu-Remaileh M, Frenkel EM, Laqtom NN, Dharamdasani V, Lewis CA, et al. NUFIP1 is a ribosome receptor for starvation-induced ribophagy. *Science* 2018;**360**:751−8.
29. Gao Y, Nihira NT, Bu X, Chu C, Zhang JF, Kolodziejczyk A, et al. Acetylation-dependent regulation of PD-L1 nuclear translocation dictates the efficacy of anti-PD-1 immunotherapy. *Nat Cell Biol* 2020;**22**:1064−75.
30. Wang L, Wen MY, Cao XT. Nuclear hnRNPA2B1 initiates and amplifies the innate immune response to DNA viruses. *Science* 2019;**365**:eaav0758.
31. Li LX, Friedrichsen HJ, Andrews S, Picaud S, Volpon L, Ngeow K, et al. A TFEB nuclear export signal integrates amino acid supply and glucose availability. *Nat Commun* 2018;**9**:2685.

32. Knockenhauer KE, Schwartz TU. The nuclear pore complex as a flexible and dynamic gate. *Cell* 2016;**164**:1162−71.
33. Dong XH, Biswas A, Suel KE, Jackson LK, Martinez R, Gu H, et al. Structural basis for leucine-rich nuclear export signal recognition by CRM1. *Nature* 2009;**458**:1136−41.
34. Grespin ME, Bonamy GMC, Roggero VR, Cameron NG, Adam LE, Atchison AP, et al. Thyroid hormone receptor alpha1 follows a cooperative CRM1/calreticulin-mediated nuclear export pathway. *J Biol Chem* 2008;**283**:25576−88.
35. Kemper JK, Xiao Z, Ponugoti B, Miao J, Fang S, Kanamaluru D, et al. FXR acetylation is normally dynamically regulated by p300 and SIRT1 but constitutively elevated in metabolic disease states. *Cell Metabol* 2009;**10**:392−404.
36. Inuzuka H, Gao DM, Finley LW, Yang W, Wan LX, Fukushima H, et al. Acetylation-dependent regulation of Skp2 function. *Cell* 2012;**150**:179−93.
37. Frankenberg T, Miloh T, Chen FY, Ananthanarayanan M, Sun AQ, Balasubramaniyan N, et al. The membrane protein ATPase class I type 8B member 1 signals through protein kinase C zeta to activate the farnesoid X receptor. *Hepatology* 2008;**48**:1896−905.
38. Yang PH, Xu C, Reece EA, Chen X, Zhong JX, Zhan M, et al. Tip60- and sirtuin 2-regulated MARCKS acetylation and phosphorylation are required for diabetic embryopathy. *Nat Commun* 2019;**10**:282.
39. Tang Y, Zhao WH, Chen Y, Zhao YM, Gu W. Acetylation is indispensable for p53 activation. *Cell* 2008;**133**:612−26.
40. Margiola S, Gerecht K, Muller MM. Semisynthetic 'designer' p53 sheds light on a phosphorylation-acetylation relay. *Chem Sci* 2021;**12**:8563−70.
41. Chen D, Xia SY, Zhang RK, Li YC, Famulare CA, Fan H, et al. Lysine acetylation restricts mutant IDH2 activity to optimize transformation in AML cells. *Mol Cell* 2021;**81**:3833−47.e11.
42. Milne JC, Lambert PD, Schenk S, Carney DP, Smith JJ, Gagne DJ, et al. Small molecule activators of SIRT1 as therapeutics for the treatment of type 2 diabetes. *Nature* 2007;**450**:712−6.
43. Li M, Hong WX, Hao CZ, Li LY, Xu HH, Li P, et al. Hepatic stellate cell-specific deletion of SIRT1 exacerbates liver fibrosis in mice. *Biochim Biophys Acta, Mol Basis Dis* 2017;**1863**:3202−11.
44. Li M, Hong WX, Hao CZ, Li LY, Wu DM, Shen AG, et al. SIRT1 antagonizes liver fibrosis by blocking hepatic stellate cell activation in mice. *FASEB J* 2018;**32**:500−11.
45. Zhou JY, Huang NN, Guo YT, Cui S, Ge CL, He QX, et al. Combined obeticholic acid and apoptosis inhibitor treatment alleviates liver fibrosis. *Acta Pharm Sin B* 2019;**9**:526−36.
46. Zhang QG, Han D, Wang RM, Dong Y, Yang F, Vadlamudi RK, et al. C terminus of Hsc70-interacting protein (CHIP)-mediated degradation of hippocampal estrogen receptor-alpha and the critical period hypothesis of estrogen neuroprotection. *Proc Natl Acad Sci U S A* 2011;**108**:E617−24.
47. Samant RS, Livingston CM, Sontag EM, Frydman J. Distinct proteostasis circuits cooperate in nuclear and cytoplasmic protein quality control. *Nature* 2018;**563**:407−11.
48. Li MY, Brooks CL, Wu-Baer F, Chen DL, Baer R, Gu W. Mono- *versus* polyubiquitination: differential control of p53 fate by Mdm2. *Science* 2003;**302**:1972−5.
49. Blus BJ, Koh J, Krolak A, Seo HS, Coutavas E, Blobel G. Allosteric modulation of nucleoporin assemblies by intrinsically disordered regions. *Sci Adv* 2019;**5**:eaax1836.
50. Han SJ, Jung SY, Wu SP, Hawkins SM, Park MJ, Kyo S, et al. Estrogen receptor beta modulates apoptosis complexes and the inflammasome to drive the pathogenesis of endometriosis. *Cell* 2015;**163**:960−74.
51. Green DR, Kroemer G. Cytoplasmic functions of the tumour suppressor p53. *Nature* 2009;**458**:1127−30.
52. Liu YS, Beyer A, Aebersold R. On the dependency of cellular protein levels on mRNA abundance. *Cell* 2016;**165**:535−50.
53. Li FL, Liu JP, Bao RX, Yan G, Feng X, Xu YP, et al. Acetylation accumulates PFKFB3 in cytoplasm to promote glycolysis and protects cells from cisplatin-induced apoptosis. *Nat Commun* 2018;**9**:508.
54. Li T, Diner BA, Chen J, Cristea IM. Acetylation modulates cellular distribution and DNA sensing ability of interferon-inducible protein IFI16. *Proc Natl Acad Sci U S A* 2012;**109**:10558−63.
55. Tan W, Jiang P, Zhang WJ, Hu ZH, Lin SF, Chen LL, et al. Post-transcriptional regulation of *de novo* lipogenesis by glucose-induced *O*-GlcNAcylation. *Mol Cell* 2021;**81**:1890−904.e7.
56. Fang S, Tsang S, Jones R, Ponugoti B, Yoon H, Wu SY, et al. The p300 acetylase is critical for ligand-activated farnesoid X receptor (FXR) induction of SHP. *J Biol Chem* 2008;**283**:35086−95.
57. Zhao Q, Liu F, Cheng Y, Xiao XR, Hu DD, Tang YM, et al. Celastrol protects from cholestatic liver injury through modulation of SIRT1−FXR signaling. *Mol Cell Proteomics* 2019;**18**:520−33.
58. Alshehri AS, El-Kott AF, El-Kenawy AE, Khalifa HS, AlRamlawy AM. Cadmium chloride induces non-alcoholic fatty liver disease in rats by stimulating miR-34a/SIRT1/FXR/p53 axis. *Sci Total Environ* 2021;**784**:147182.
59. Gao Z, Zhang JC, Wei L, Yang XP, Zhang Y, Cheng B, et al. The protective effects of imperatorin on acetaminophen overdose-induced acute liver injury. *Oxid Med Cell Longev* 2020;**2020**:8026838.
60. Kulkarni SR, Soroka CJ, Hagey LR, Boyer JL. Sirtuin 1 activation alleviates cholestatic liver injury in a cholic acid-fed mouse model of cholestasis. *Hepatology* 2016;**64**:2151−64.
61. Blokker BA, Maijo M, Echeandia M, Galduroz M, Patterson AM, Ten A, et al. Fine-tuning of sirtuin 1 expression is essential to protect the liver from cholestatic liver disease. *Hepatology* 2019;**69**:699−716.
62. Garcia-Rodriguez JL, Barbier-Torres L, Fernandez-Alvarez S, Gutierrez-de Juan V, Monte MJ, Halilbasic E, et al. SIRT1 controls liver regeneration by regulating bile acid metabolism through farnesoid X receptor and mammalian target of rapamycin signaling. *Hepatology* 2014;**59**:1972−83.
63. Liu PY, Chen CC, Chin CY, Liu TJ, Tsai WC, Chou JL, et al. E3 ubiquitin ligase Grail promotes hepatic steatosis through SIRT1 inhibition. *Cell Death Dis* 2021;**12**:323.
64. Han X, Ding C, Sang XN, Peng MY, Yang Q, Ning Y, et al. Targeting sirtuin1 to treat aging-related tissue fibrosis: from prevention to therapy. *Pharmacol Ther* 2022;**229**:107983.